Spring 2024

Folding and Embedding Cubical Complexes

Skye Rothstein
Bard College

Folding and Embedding Cubical Complexes

A Senior Project submitted to
The Division of Science, Mathematics, and Computing
of
Bard College

by
Skye Rothstein

Annandale-on-Hudson, New York
May, 2024

Abstract

In this project we study the folding properties of several special classes of cubical complexes. First, we look at polyominoids, which are arrangements of congruent squares in 3-space, glued edge-to-edge at 90° and 180° angles. We construct and analyze the mechanical configuration space for n-cell polyominoids, which is a graph with vertex set given by all n-cell polyominoids, where two vertices are connected by an edge if you can transform one into the other by one hinge movement. For $n = 4$, we provide a complete characterization, and we also prove some structural properties for all n. Next, we study fenestrated polyominos, which are arrangements of congruent squares in 2-space, glued edge-to-edge, in such a way that fenestrations (i.e. holes) are contained in the figure. We enumerate folding patterns which, when assigned to the edges of a fenestrated polyomino, collapse its fenestrations by folding it into a 3D polyominoid. Lastly, we realize 4D hypercubes as surfaces by following precise coloring rules and removing faces incompatible with those rules. We find that under a specific quotienting operation relevant to supersymmetry physics, the 4-cube becomes un-embeddable in 3-space using non-intersecting quadrilateral flats.

Contents

Acknowledgments

A moment of gratitude.

I would like to thank my research advisors Chuck Doran and Erika Roldan for their guidance. Lauren Rose, for her kindness, mentorship, and confidence in me. Nate Harman and Josh Mundinger, for supervising my very first research project and curating a working environment that helped me believe I had a place in the world of math. Cheyne Glass, for his enthusiasm and openness, for being a steadfast ally in mathematically trying times. Karla Rothstein and Salvatore Perry for their lifelong support of my health and growth, for all the games of charades and bananagrams, for the warm summer nights on the terrace, for holding me close. I have so many people to thank for sharing their joy, love, and companionship with me. Hana Yoshikawa, for the otters and quails and endless affection. Claire Sullivan, for refuge and embrace. Lavender Johnson, for cohabitating with me, for company through all the throes of life. Erik Brodsky, for the party bus, for a bit of lightheartedness in the strangest times. Lola Vescovo, for her infectious determination to not be crushed by absurd expectations. Josh Krienke, for game nights, inextinguishable joviality, and that one time we wore the same color shirt. Thanasis Kostikas, for the night we stood at the end of my driveway cackling about cryptocurrency long after we planned to part ways. Sasha Wald, for our childhood together. Kace Colby, for his outrageous sleeping habits, unshakable calm, and spot-on impressions. Neil Bhatia, for his honesty (when he's not gaslighting, gatekeeping, and girlbossing). Alexis Joseph, for the late summer night we walked across Brooklyn to get plums and stayed up cooking with no worries in our hearts. Nahfila Ali, for being up at all hours, just a text away even when I'm halfway across the world. Ham White, for an abundance of laughter, for standing outside in the cold with me until our toes froze the first time we met, for understanding the unexplainable. Oliver Vanderploeg, for adventuring with me, for banana pancakes and chocolate-date smoothies, for walks through the falling snow, for teaching me to have faith in myself. Joel Towers, for the countless dinners and cozy evenings, for being a reason I treasure my brief returns to Brooklyn.

Ada Vargas, for being the core of my second family and home. And Lenore Perry and Dalitta Rothstein for their grandmotherly affection.

1
Introduction

In this paper, we investigate folding properties of three special classes of cubical complexes.

Definition 1.0.1. A *cubical complex* is a set composed of points, line segments, squares, cubes, and their higher dimensional counterparts.

We will study polyominoes, polyominoids, and hypercubes, which live in 2, 3, and 4 dimensions, respectively.

Definition 1.0.2. An *n-cell polyomino* is a connected 2D geometric figure formed by joining n congruent squares edge-to-edge.

Treating edges as hinges, we manipulate these objects through a series of hinge movements of 90° or 180° rotation to obtain 3D polyominoids, whose vertices live in a cubical lattice.

Definition 1.0.3. An *n-cell polyominoid* is a connected 3D geometric figure, formed by joining n congruent squares edge-to-edge at 90° or 180° angles.

Example 1.0.4. A 6-cell 2D polyomino being folded into a 3D polyominoid through a series of 4 hinge movements is pictured below in Figure 1.0.1.

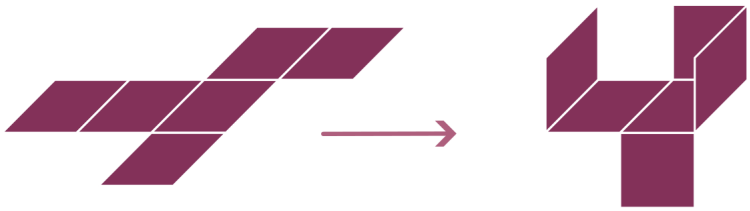

Figure 1.0.1: Folding a 6-cell 2D polyomino into a 3D polyominoid

Definition 1.0.5. Two polyominoids are *friends* if one can be transformed into the other through one hinge movement of 90° or 180°.

A hinge movement is defined explicitly in the following section.

Definition 1.0.6. The *mechanical configuration space for n-cell polyominoids* is a graph with vertex set given by all n-cell polyominoids and edge set given by all friendships between them.

We explicitly construct the mechanical configuration space for 4-cell polyominoids and present several theorems describing the structure and growth of the mechanical polyominoid configuration space as $n \to \infty$. We make progress toward answering the question, given two n-cell polyominoids, can we know whether they are connected by a series of hinge movements?

Example 1.0.7. A subgraph of the 4-cell mechanical configuration space is pictured in Figure 1.0.2. There exist 47 other 4-cell polyominoids, none of which can be transformed into these 7 through a series of hinge movements. This subgraph is an isolated component of the configuration space.

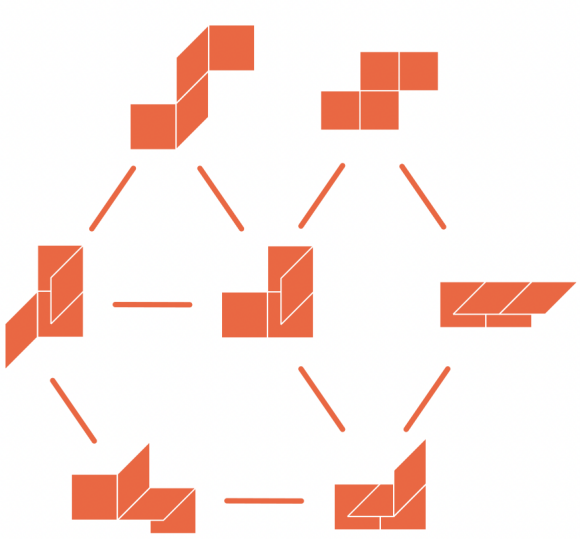

Figure 1.0.2: A subgraph of the 4-cell configuration space

Next, we begin an investigation in folding special classes of 2D polyominoes into 3D polyominoids using rigid origami.

Definition 1.0.8. A *fenestration* is a transparent square, or set of adjacent congruent transparent squares arranged edge-to-edge.

Informally, a fenestration can be understood as a hole.

Definition 1.0.9. A *fenestrated polyomino* is a polyomino that contains one or more fenestrations.

Example 1.0.10. Three examples of fenestrated polyominoes are pictured in Figure 1.0.3. The first is an 8-cell polyomino containing a 1-cell fenestration. The second is a 12-cell polyomino containing a 3-cell fenestration. The third is a 14-cell polyomino containing two 1-cell fenestrations.

Figure 1.0.3: Fenestrated polyominoes

We observe that there exist many fenestrated polyominoes for which a folding pattern can be assigned to its edges which closes all fenestrations. Such a fenestrated 2D polyomino can be developed into a non-fenestrated 3D polyominoid which is topologically equivalent to a disc. An example of a fenestrated polyomino being "discified" is shown in Figure 1.0.4 for a 21-cell polyomino containing 4 fenestrations.

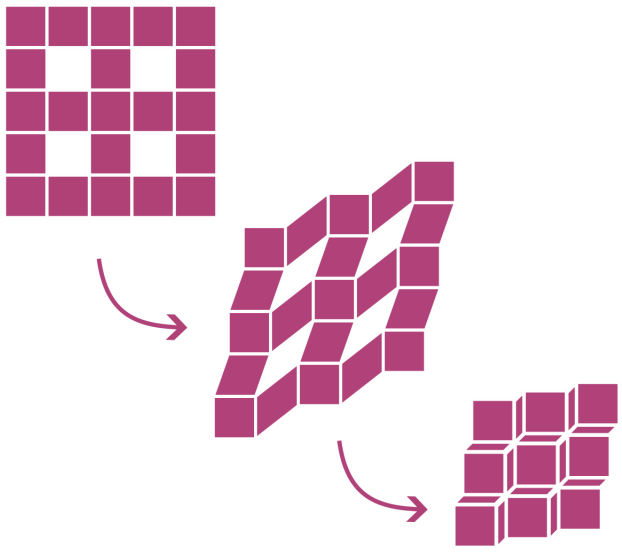

Figure 1.0.4: "Discification" of a fenestrated polyomino

We then expand from the local to global picture, constructing "unbounded" polyominos using periodic patterns of fenestrations.

Definition 1.0.11. A *periodic pattern* in the plane is a design having the following property: there exists a finite region and two linearly independent translations such that the set of all images of the region when acted on by the group generated by these translations produce the original design.

Definition 1.0.12. An *unbounded periodically fenestrated polyomino* is a 2D polyomino constructed from an infinite number of squares such that its fenestrations are arranged in a planar periodic pattern.

We pair an unbounded periodically fenestrated 2D polyomino with a folding pattern which collapses all of its fenestrations to produce an unbounded non-fenestrated 3D polyominoid. Note that the folding pattern must possess the exact same periodic pattern as the given polyomino. We present several examples of folding unbounded fenestrated 2D polyominoes into unbounded non-fenestrated 3D polyominoids, working toward answering the question: for which arrangements of fenestrations on a 2D polyomino is it impossible to assign a folding pattern which collapses them all?

Finally, we study a distinct higher dimensional topic – embedding hypercubes in 3-space using non-intersecting quadrilateral flats. The motivation for this study comes from a special class of objects from supersymmetry physics called Adinkra chromotopologies.

Definition 1.0.13. An n-dimensional Adinkra *topology* is a finite connected simple graph G such that G is bipartite and n-regular (every vertex has exactly n incident edges).

Definition 1.0.14. An n-dimensional Adinkra *chromotopology* is an Adinkra topology G such that the following holds:

1. Edges of G are colored by n colors, such that every vertex is incident to exactly one edge of each color.

2. For any distinct i and j, the edges in $E(G)$ with colors i and j form a disjoint union of 4-cycles.

It is known, from [CS1D], that hypercubes quotiented by doubly even codes index Adinkra chromotopologies.

Definition 1.0.15. A *doubly even code* is a subspace of $\mathbb{F}_2^n$ such that, for each element in the subspace (i.e. each sequence of 0's and 1's, or "codeword"), the number of non-zero entries in the codeword is divisible by 4.

In [GSA1], it is shown that Adinkra chromotopologies have canonical realizations as Riemann surfaces. We focus on the 4-cube quotiented by the code generated by 1111, shown in Figure 1.0.5 below. While topologically a torus, we show this object is not embeddable in $\mathbb{R}^3$ using non-intersecting quad flats.

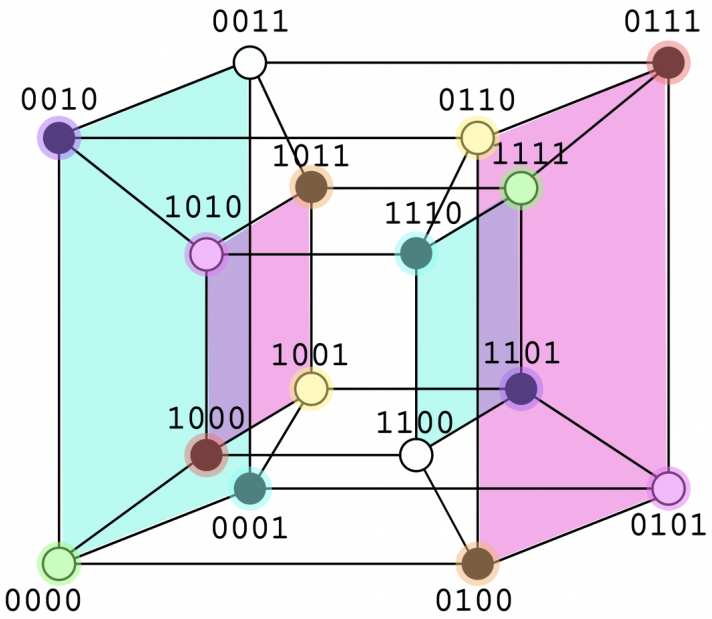

Figure 1.0.5: The 4-cube quotiented by the code generated by 1111, with all 8 vertex identifications shown and 2 of 8 face identifications shown

2
Mechanically Configured Polyominoids

2.1 Intro to Polyominoids

Enumerating 2D polyominoes is a problem which has relevance dating to antiquity. The enumeration of 5-cell polyominoes (also known as pentominoes) was documented as an observation of an ancient master of the Chinese game Go, which was invented at least 4000 years ago and is the oldest board game still played today. These mathematical objects were named and popularized by Solomon Golomb in 1953 at a talk to the Harvard Mathematics Club. He later wrote a book about them titled *Polyominoes: Puzzles, Patterns, Problems, and Packings* [SG94].

Polyominoes of sizes 1 through 4 are enumerated below in Figure 2.1.1. There exist 12 polyominoes of size 5.

Figure 2.1.1: All polyominoes of sizes 1 through 4

We will consider all squares to have side length 1 and all vertices to have integer coordinates. An example of a 9-cell polyominoid with all vertices clearly living on points of the integer lattice is shown in Figure 2.1.2.

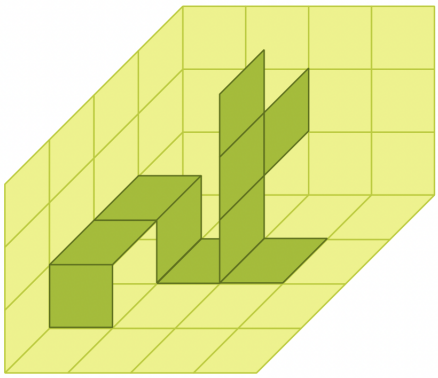

Figure 2.1.2: A 9-cell polyominoid

Definition 2.1.1. Two polyominoids P and P' are considered to be *isomorphic* if we can move P to P' by a sequence of rotations, translations, and axial reflections.

Example 2.1.2. Three isomorphic polyominoids under these transformations are shown in Figure 2.1.3. A reflection takes us from the first to the second, and a rotation takes us from the second to the third.

Figure 2.1.3: Three isomorphic polyominoids under rotations and reflections

Let P_n denote the set of isomorphism classes of n-cell polyominoids. P_1 through P_3 are shown in Figure 2.1.4.

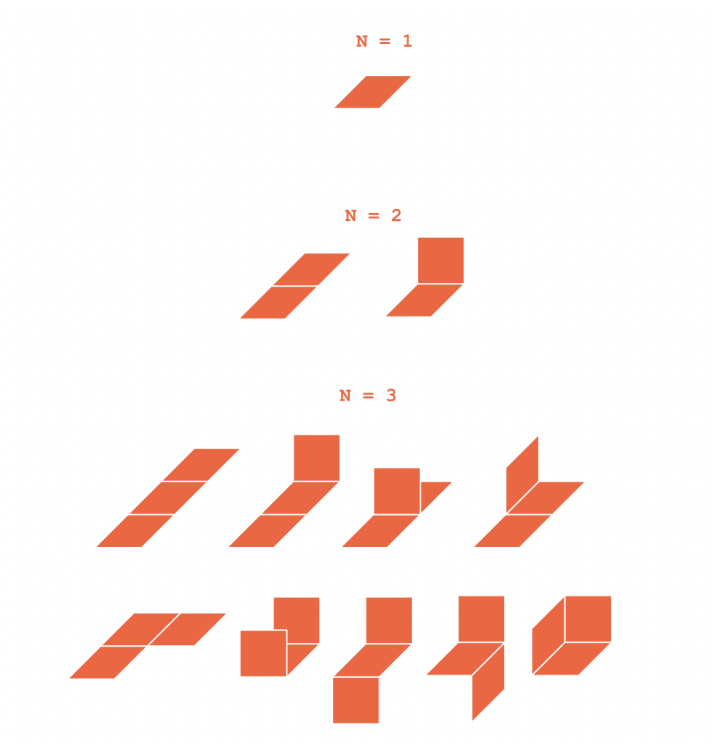

Figure 2.1.4: The isomorphism classes P_1, P_2, P_3

In 2002, Joseph Myers enumerated n-cell polyominoids, calculating $|P_n|$ up to $n = 12$ and published the sequence on the OEIS entry A075679. These values are shown in Figure 2.1.5. In 2016, John Mason constructed images for the isomorphism classes of P_n up to $n = 5$ and added these graphics to OEIS entry A075679.

n	$\lvert P_n \rvert$
1	1
2	2
3	9
4	54
5	448
6	4650
7	53611
8	655033
9	8259635
10	106371085
11	1391032357
12	18412269694

Figure 2.1.5: Enumeration of n-cell polyominoids

We now define a hinge movement, which, informally, is rotating one or more squares 90° or 180° around an edge.

Example 2.1.3. Three valid hinge movements are pictured in Figure 2.1.6

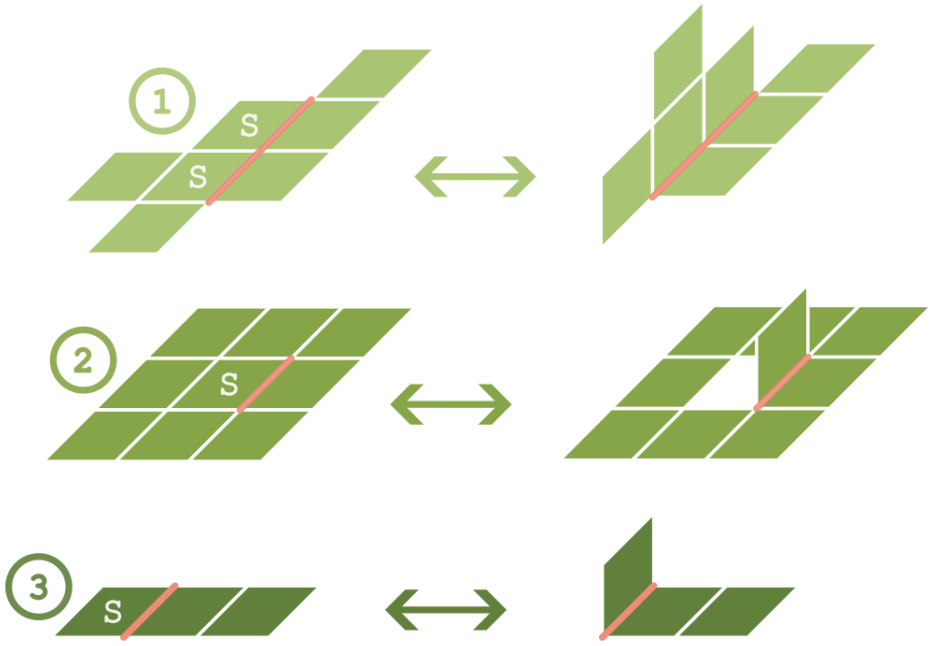

Figure 2.1.6: Three valid hinge movements

Definition 2.1.4. A *hinge movement* can occur around a "single-hinge" (length 1), or a "multi-hinge" (length ≥ 2) and is uniquely defined by four values (H, S, M, θ).

A hinge-movement around a "single-hinge" is constructed as follows.

1. Choose an edge H to be our hinge. H must have 2 or 3 faces incident to it.
2. Choose a square S adjacent to H.
3. Choose a sub-polyominoid M containing S.
4. Choose an angle θ to be 90° or 180°.
5. Rotate M around H by angle θ.
6. If the result is connected and has not collided with itself in the process of rotation, (H, S, M, θ) is a valid hinge movement.

A hinge-movement around a "multi-hinge" is constructed identically except that H is a set of 2 or more adjacent parallel edges (all of degree 2 or 3), and S is a set of adjacent squares, all incident to H.

Example 2.1.5. Two invalid hinge movements are demonstrated in Figure 2.1.7. Movement #4 is invalid because it causes the polyominoid to collide with itself. Movement #5 is invalid because the result of the movement is disconnected.

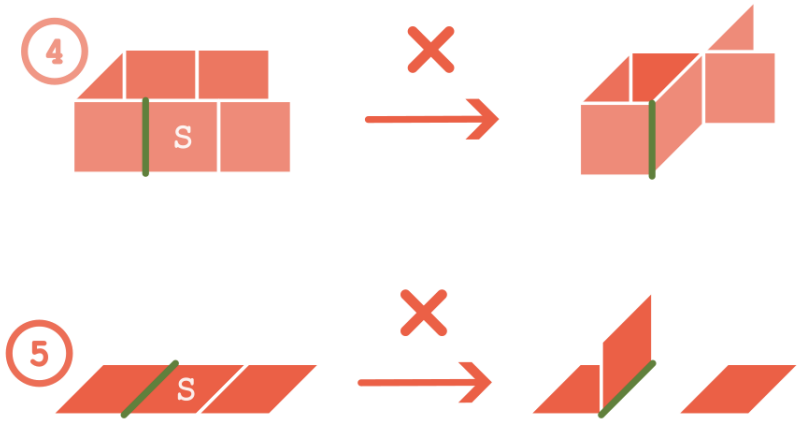

Figure 2.1.7: Two invalid hinge movements

Definition 2.1.6. Two polyominoids are *friends* if one can be transformed into the other through one hinge movement of 90° or 180°.

Example 2.1.7. The two polyominoids in P_2, shown in Figure 2.1.4 are friends.

Definition 2.1.8. The *mechanical configuration space for n-cell polyominoids*, denoted $\mathbb{G}_n$, is a graph with vertex set given by all n-cell polyominoids and edge set given by all friendships between them.

A subgraph of the mechanical configuration space for 4-cell polyominoids, denoted $\mathbb{G}_4$, is shown in Figure 2.1.8.

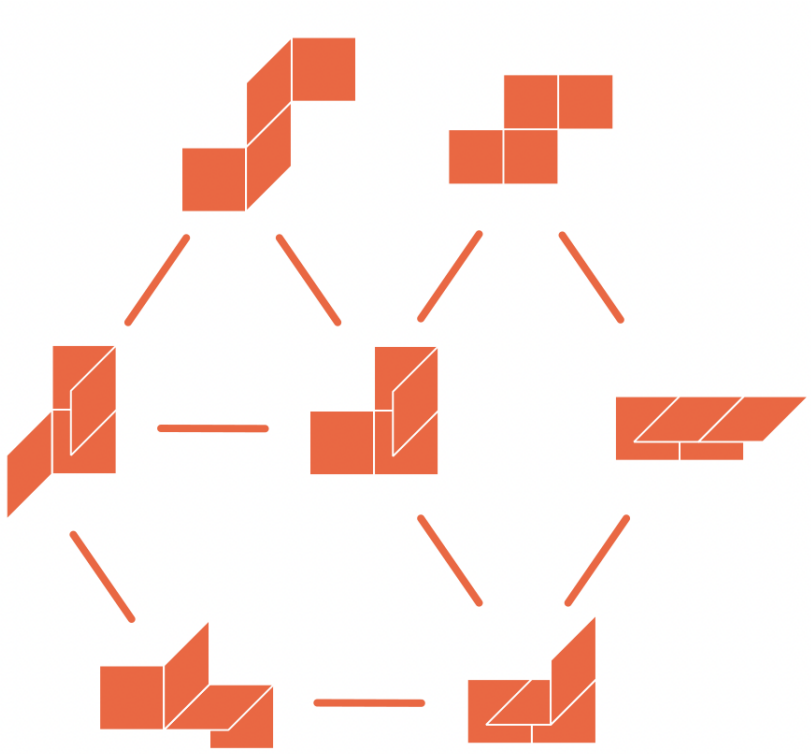

Figure 2.1.8: A subgraph of $\mathbb{G}_4$

2.2 A Complete Mechanical Polyominoid Configuration Space for n=4

Theorem 2.2.1. *The mechanical configuration space for 4-cell polyominoids, $\mathbb{G}_4$, is a graph with 54 vertices which has exactly 5 disjoint components.*

Proof. From Myers' enumeration (see Figure 2.1.5), we know $|P_4| = 54$, thus we have 54 vertices. The 5 components are constructed in Figures 2.2.1, 2.2.2, and 2.2.3. This was a brute force construction in which the 54 possible 4-cell polyominoid configurations were sorted into sub-families before checking every possible friendship within each sub-family. This result was later computationally verified by John Mason. □

We now describe these 5 components in more detail.

Definition 2.2.2. The *"snake" family* consists of all elements which can be reduced to a linear $1 \times N$ strip through a series of hinge movements.

All friendships between elements of the snake family of $\mathbb{G}_4$ are shown in Figure 2.2.1. This is one of five disjoint components in $\mathbb{G}_4$.

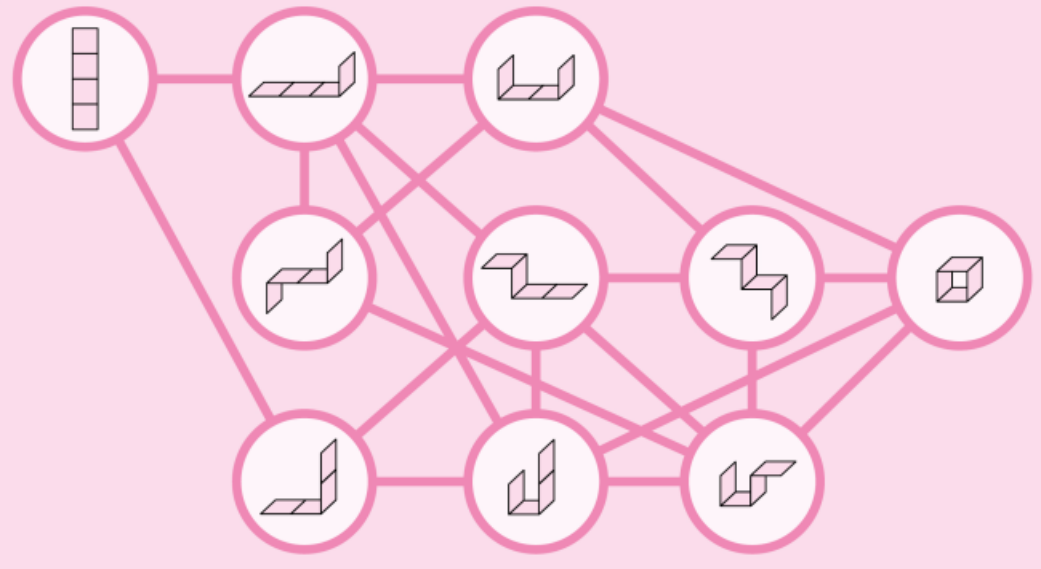

Figure 2.2.1: The snake component of $\mathbb{G}_4$

We utilize the special linear structure of the elements in the snake component in Section 2.3 to prove the number of elements in this component grows at an exponential rate with respect to N.

We show 3 more disjoint components named the "chair," "book," and "lonely" families in Figure 2.2.2.

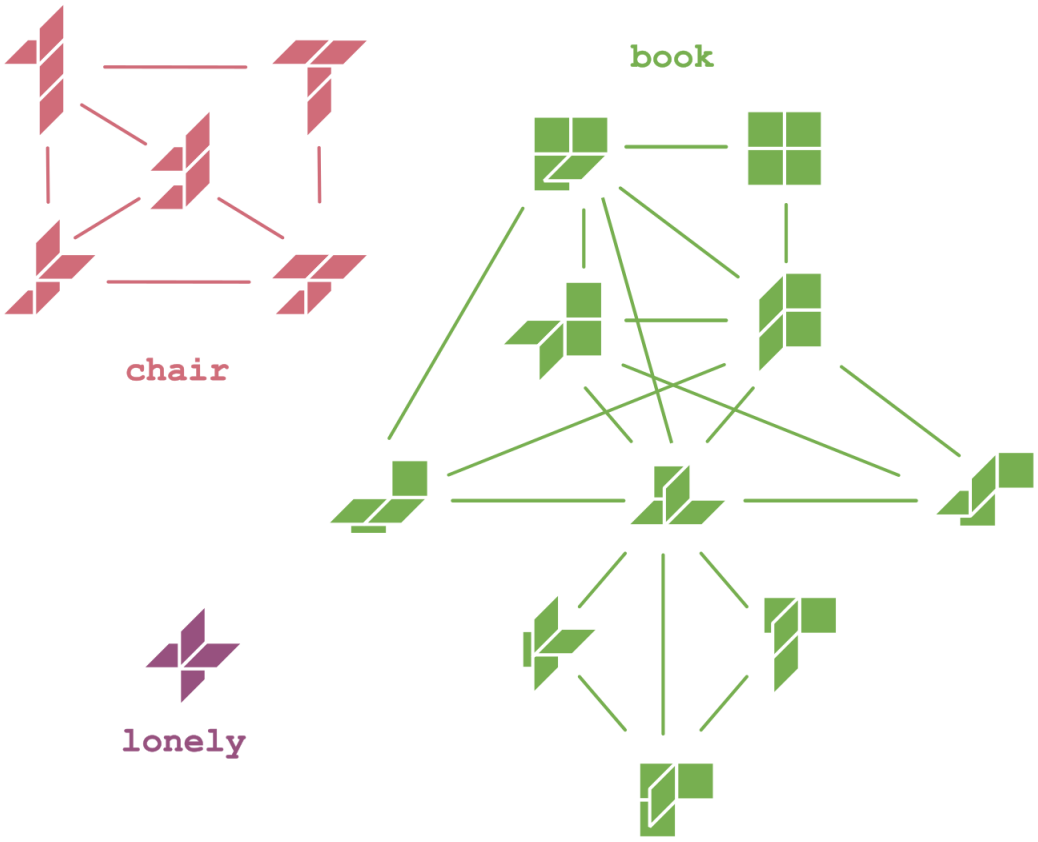

Figure 2.2.2: Three sub-families of the $\mathbb{G}_4$ graph, each their own disjoint component of the configuration space

The last component is called the "great family gathering" because it consists of 3 sub-families which overlap at only 3 special nodes. We see the 3 subgraphs "squiggle," "cowboy," and "leg" shown in Figure 2.2.3 and nodes which connect to one or two of the 3 special portals have the associated colors in their background.

Definition 2.2.3. A *planar polyominoid* has all hinges set at 180° angles.

Remark 2.2.4. The set of planar n-cell polyominoids is equal to the set of n-cell polyominoes.

Each of the three sub-families, "squiggle, "cowboy," and "leg" are named after the appearance of their planar polyominoid.

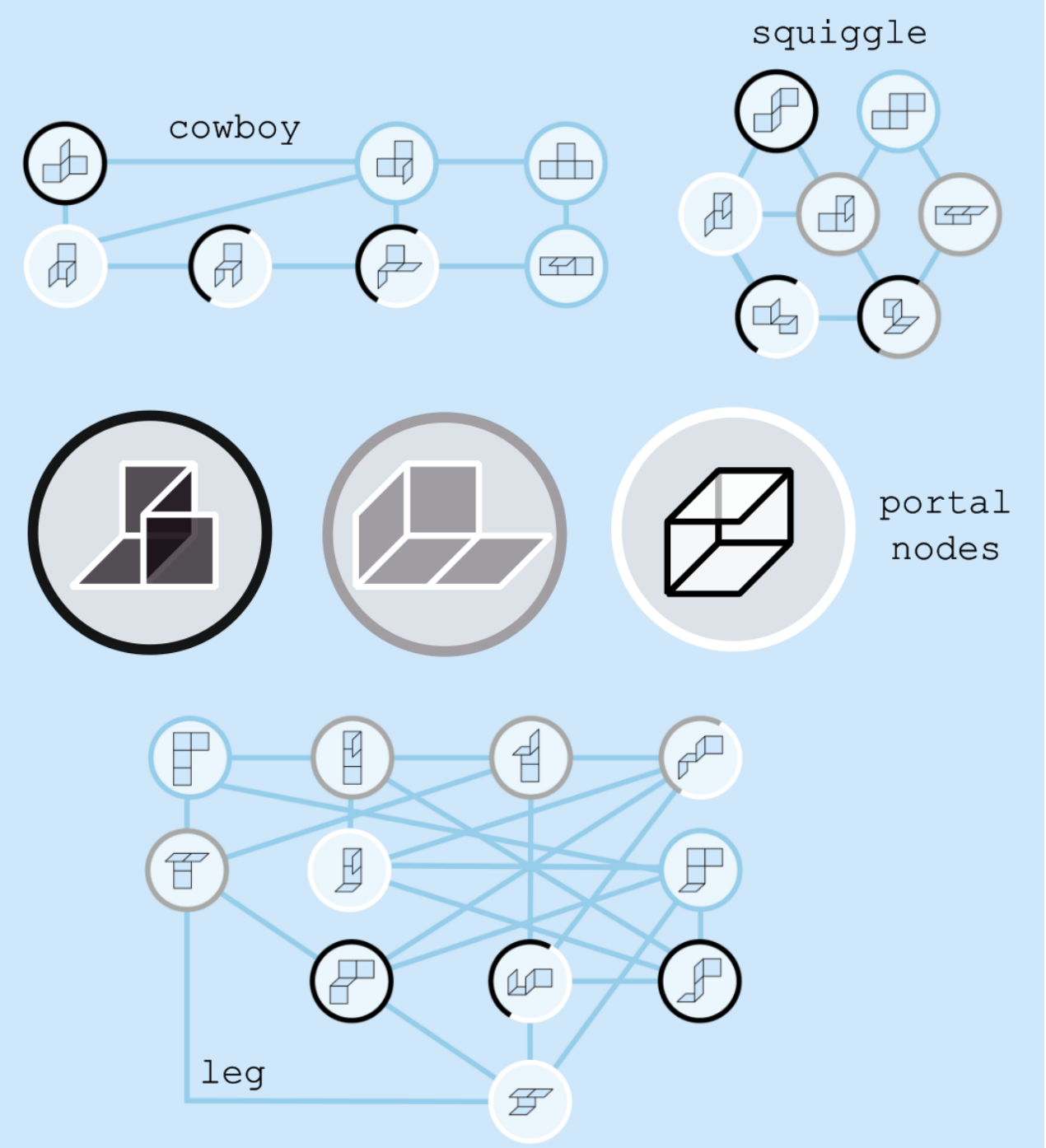

Figure 2.2.3: Three sub-families which make up the last component of $\mathbb{G}_4$

Many questions can now be asked about $\mathbb{G}_n$ for arbitrary n, which is the subject of the next section.

1. How many disjoint components does $\mathbb{G}_n$ have?

2. How big are these components?

3. Given two n-cell polyominoids, can we decide whether they live in the same component?

2.3 Size of Snake Component

We first address question 2 with an investigation into the size of a particular component of $\mathbb{G}_n$ we call the "snake" component due to the linear nature of its elements.

Definition 2.3.1. A *linear* polyominoid has all edges parallel

Remark 2.3.2. A *linear* polyominoid can be easily drawn in 2D as a walk on the integer lattice $\mathbb{Z}^2$ by projecting down one dimension. An example is given in Figure 2.3.1.

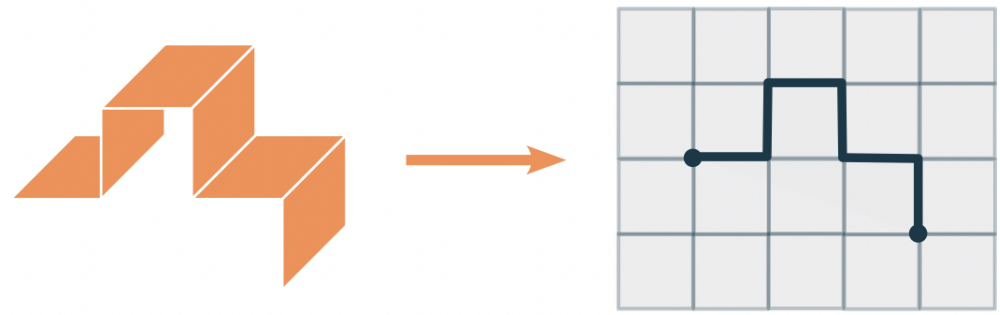

Figure 2.3.1: A linear polyominoid and its associated lattice walk

Definition 2.3.3. The *"$1 \times n$ configuration"* is a strip of n squares.

Definition 2.3.4. A polyominoid is a member of the *snake component* if it can be transformed into the linear $1 \times n$ configuration through a series of hinge movements.

Remark 2.3.5. Note that all elements of the snake component must be linear.

Remark 2.3.6. The snake component is unexpectedly large for arbitrary n. It includes many complex configurations that can eventually be unfolded to a simple line of squares.

Example 2.3.7. An element of $\mathbb{G}_{14}$ is shown below in Figure 2.3.2 for which it is not immediately obvious that it belongs to the snake component. Its explicit unfolding into a snake shape is demonstrated.

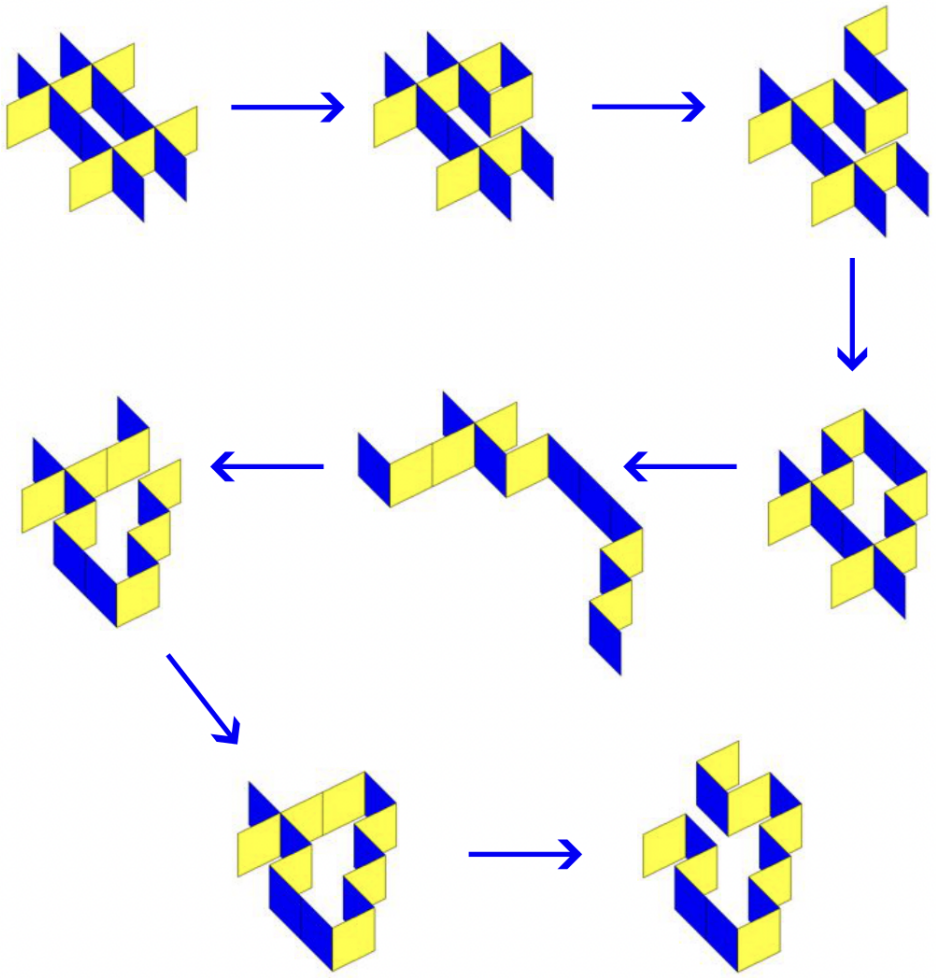

Figure 2.3.2: An unfolding of a linear polyominoid in $\mathbb{G}_{14}$ into a snake (figure made in collaboration with John Mason)

Example 2.3.8. For contrast, an example of a non-linear polyominoid from $\mathbb{G}_{14}$ is shown in Figure 2.3.3. It cannot be represented as a walk on the integer lattice.

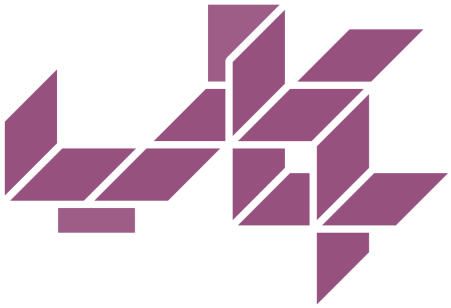

Figure 2.3.3: A non-linear polyominoid in $\mathbb{G}_{14}$

Theorem 2.3.9. *The number of elements in the snake component of $\mathbb{G}_n$ grows at an exponential rate with respect to n.*

Proof. Let $Snakes(n)$ denote the number of snakes in the snake component of $\mathbb{G}_n$.

We will utilize the correspondence between a linear polyominoid and a walk as pictured in Figure 2.3.1. Let W_n be the set of lattice walks of length n which travel strictly up and right. Let elements which are identical under reflection over the $y = x$ line or under rotations by 180° be considered isomorphic. Note that these transformations preserve the up-and-right structure of our lattice walks. Thus each element of W_n represents a snake in $\mathbb{G}_n$. Not all snakes can be represented by walks which travel strictly up and right, some turn back and touch themselves, so $|W_n| < Snakes(n)$.

Thus, the cardinality of the set $|W_n|$ provides a lower bound on the number of elements in the snake component $Snakes(n)$.

In 1961, Eden provided a lower bound for $|W_n|$ in Section 2 of [ME61]. Every time n is incremented by 1, we have two choices: go up or right. Thus we have 2^n walks. After accounting for reflection over the $y = x$ diagonal and rotations by 180°, our count is reduced by a factor of 4, and thus $|W_n| > 2^{n-2}$.

We have $Snakes(n) > |W_n| > 2^{n-2}$. Therefore, the number of elements in the snake component of $\mathbb{G}_n$ grows at an exponential rate with respect to n. □

2.4 Conjectured Structure of Configuration Spaces

After constructing the configuration space for $n = 4$ and finding that $\mathbb{G}_4$ has 5 components, we wondered, as n increased, would we find a highly connected graph that merges to a single component? Or a highly disjoint graph with a growing number of distinct components?

We found that both of these behaviors are present. While the snake component grows exponentially with n, we also see many smaller components which we call "stuck" when no hinge movements are possible and "almost stuck" when only a small number of hinge movements are possible, none of which increase or decrease the number of holes present in the polyominoid.

Definition 2.4.1. A hinge is *fully saturated* if all four adjacent squares are occupied.

Definition 2.4.2. A *stuck* polyominoid must have all hinges "fully saturated".

Remark 2.4.3. Every *stuck* polyominoid represents an isolated component of $\mathbb{G}_n$.

Example 2.4.4. Examples of stuck polyomonoids in $\mathbb{G}_4$, $\mathbb{G}_7$, $\mathbb{G}_{12}$ are shown in Figure 2.4.1.

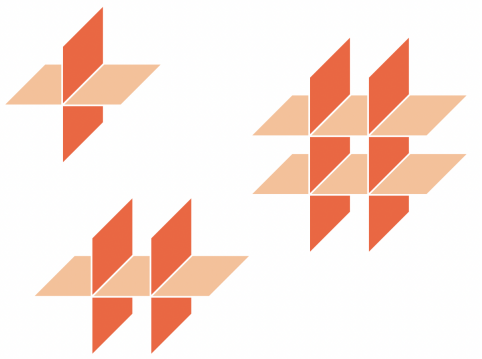

Figure 2.4.1: Examples of stuck polyomonoids in $\mathbb{G}_4$, $\mathbb{G}_7$, $\mathbb{G}_{12}$

Definition 2.4.5. The *topology* of a polyominoid is given by the number of holes present.

Definition 2.4.6. An *almost stuck* polyominoid has a topology which cannot be changed by hinge movements.

An example of two almost stuck polyominoids which constitute all the elements in their component of size 2 in $\mathbb{G}_5$ is shown in Figure 2.4.2

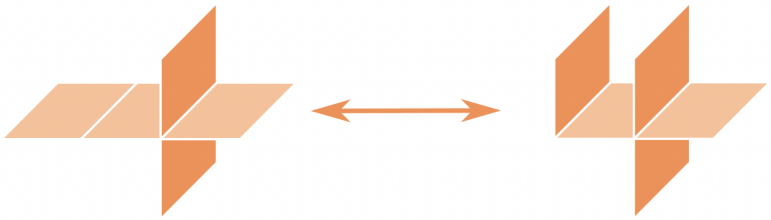

Figure 2.4.2: Almost stuck polyominoids in $\mathbb{G}_5$

We now present a conjecture about the structure of connected components of $\mathbb{G}_n$, illustrated in Figure 2.4.3.

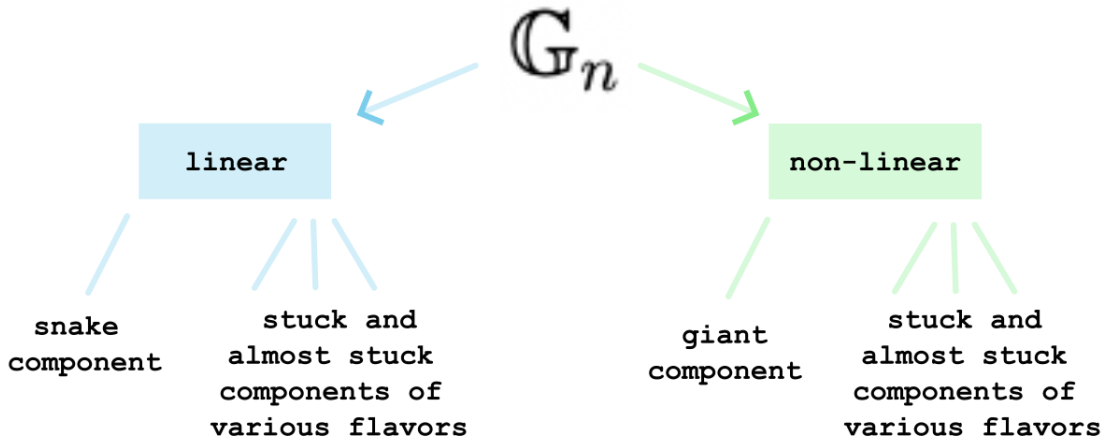

Figure 2.4.3: Conjectured structure of $\mathbb{G}_n$

Conjecture 2.4.7. *A polyominoid whose topology can be changed through a series of hinge movements must live in the snake component (if linear) or giant component (if non-linear). Otherwise, the topology of a polyominoid is fixed and it must live in a "stuck" or "almost stuck" component.*

An immediate corollary of this result would be the following:

Conjecture 2.4.8. *Given two n-cell polyominoids, if one has alterable topology and one does not, they are not joined by a series of hinge movements in $\mathbb{G}_n$.*

A first step toward proving these conjectures is the following lemma.

Lemma 2.4.9. *Linear and non-linear n-cell polyominoids must live in distinct components of the configuration space* $\mathbb{G}_n$.

Proof. A non-linear polyominoid, by definition, does not have all hinges parallel. Let P be a linear polyominoid. There exist no hinge movements which will create perpindicular hinges. □

2.5 Number of Components as n goes to Infinity

We are able to prove the number of components of $\mathbb{G}_n$ grows linearly with n by constructing a family of almost stuck polyominoids we call "spiky spines" for any given $n \geq 12$. These polyominoids have very limited movement, nearly all of their hinges are "fully saturated" with a small gap which allows limited movement. Each of these "spiky spines" is a representative of a small disjoint component of the configuration space.

Theorem 2.5.1. *As* $n \to \infty$, *the number of components of* $\mathbb{G}_n$ *also trends toward infinity.*

The proof of this theorem will utilize an object we call a "spiky spine" which is defined as follows.

Definition 2.5.2. A *spiky spine* is a special polyominoid of size n formed by joining a series of crosses with one gap of length 3. The precise construction of this object for different values of $n \pmod 3$ is below.

If $n \equiv 0 \pmod 3$, attach $\frac{n-3}{3}$ sections of one horizontal and two vertical squares. Add 2 horizontal squares between the last and second-to-last vertical strut. Add 1 horizontal square on the far right end. This construction is shown for $n = 12$ in Figure 2.5.1.

Figure 2.5.1: Spiky spine construction for $n = 12$

If $n \equiv 1 \pmod 3$, attach $\frac{n-4}{3}$ sections, add 2 horizontal squares before the last strut to construct the gap. Add 2 on the far right. This construction is shown for $n = 13$ in Figure 2.5.2.

Figure 2.5.2: Spiky spine construction for $n = 13$

If $n \equiv 2 \pmod 3$, attach $\frac{n-5}{3}$ sections. Add 2 squares to create the gap. Add 2 on the far right and 1 on the far left. This construction is shown for $n = 14$ in Figure 2.5.3.

Figure 2.5.3: Spiky spine construction for $n = 14$

Proof. Fix $n \geq 12$. We will construct several "almost stuck" n-cell polyominoids using the spiky-spine construction that each represent a different connected component of $\mathbb{G}_n$ and find that the number of such polyominoids grows linearly with respect to n.

The extra two horizontal squares which create our gap of size 3 can be placed between other vertical struts to create more spiky-spine representatives of disjoint components. For example, in Figure 2.5.4, which illustrates all spiky-spine representatives for $n = 12$, we have 5 gaps between vertical struts, and after accounting for duplicates under reflection, moving our extra two squares provides us with 3 unique almost stuck polyominoids, each of which represents their own disjoint component in $\mathbb{G}_{21}$.

Let $k \equiv n \pmod 3$.

Let $v = \frac{n-3-k}{3}$ be the number of vertical struts in our spiky spine by construction.

Let $g = v - 1$ be the number of gaps in our spiky spine.

Let $s = \lceil \frac{g}{2} \rceil$ be the number of gaps, after accounting for reflections, where we can insert our extra 2 squares to create spiky spine representatives of almost stuck components of $\mathbb{G}_n$. The ceiling function is necessary to account for parity introduced by the number of gaps being even or odd.

Then $s(n) = \left\lceil \frac{\frac{n-3-k}{3}-1}{2} \right\rceil$ defines the number of distinct spiky-spines in terms of n.

See the example in Figure 2.5.4 to check that for $n = 21$, we have $\left\lceil \frac{\frac{21-3-0}{3}-1}{2} \right\rceil = 3$ spiky spine representatives.

Note that as long as $n \geq 12$, $s(n) = \left\lceil \frac{\frac{n-3-k}{3}-1}{2} \right\rceil$ provides a lower bound for the number of components in $\mathbb{G}_n$.

Observe that $s(n)$, which denotes the number of spiky spine representatives of almost stuck components, has a linear relationship with n and thus the total number of components of the configuration space $\mathbb{G}_n$ must approach infinity as $n \to \infty$.

□

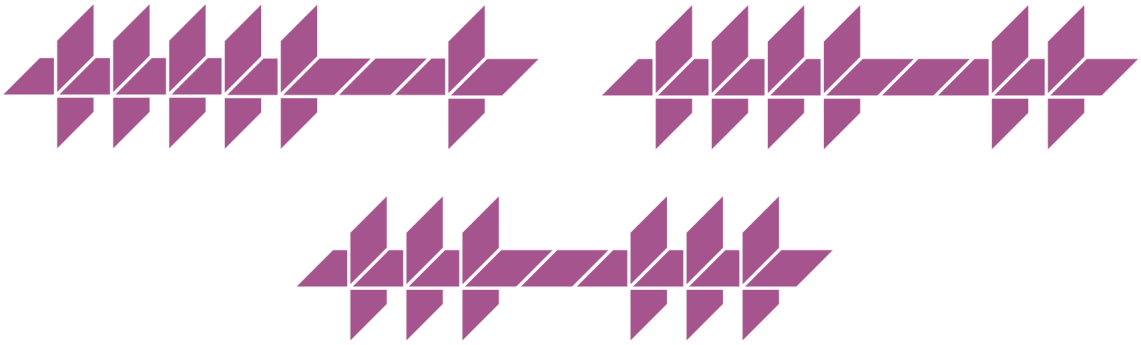

Figure 2.5.4: Three spiky spine representatives of components in $\mathbb{G}_{21}$

3
Collapsing Fenestrations through Rigid Origami

3.1 Research Question

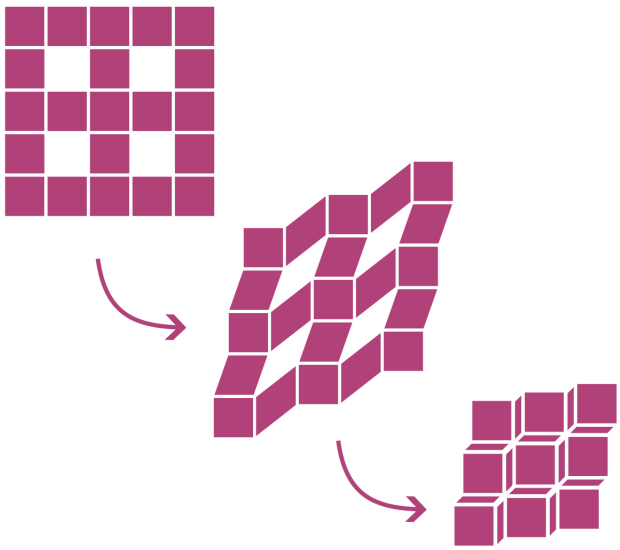

Figure 3.1.1: "discification" of a fenestrated polyomino

Definition 3.1.1. A *fenestration* is a transparent square, or set of adjacent transparent squares, surrounded by solid squares.

Informally, a fenestration can be understood as a hole.

Definition 3.1.2. A *fenestrated* polyomino is a polyomino which contains one or more fenestrations.

While experimenting with developing interesting polyominoids out of various polyomino nets in collaboration with artist Yaron Maïm, we realized that many fenestrated polyominoes can be developed into topological discs when assigned precise folding patterns which collapse all of the fenestrations originally present. One such 21-cell polyomino containing 4 fenestrations and a possible "discification" of it is shown in Figure 3.1.1.

We construct several collapsible fenestrated polyominos and work toward answering the question, for which arrangements of fenestrations is it impossible to "discify?"

We first look locally at "solo" fenestrations and enumerate how many folding patterns exist which will collapse them.

Definition 3.1.3. A *solo fenestration* is one or more transparent squares arranged edge-to-edge and surrounded by a width-1 border strip of solid squares.

Polyominoes are traditionally finite objects, but we also look at an infinite analog, called "unbounded" polyoiminoes, which we build with a periodic arrangement of fenestrations. We present examples of collapsible and non-collapsible unbounded periodically fenestrated polyominoes. For the collapsible examples, we explicitly construct a folding pattern which collapses all fenestrations.

3.2 The Local Picture: Collapsing Fenestrations Through Folding

By first focusing on the local picture – enumerating and describing all possible folding patterns which collapse n-cell fenestrations for low n on a width-1 strip surrounding the fenestration, we produce tools for constructing larger fenestrated polyominoes and determining whether they are collapsible.

Folding notation in successive figures is as follows. A solid line denotes a mountain fold, meaning the isolated hinge laid flat will press upward out of the plane. A dashed line denotes a

valley fold, meaning the isolated hinge will sink below the plane it originally lay on, as shown in Figure 3.2.1.

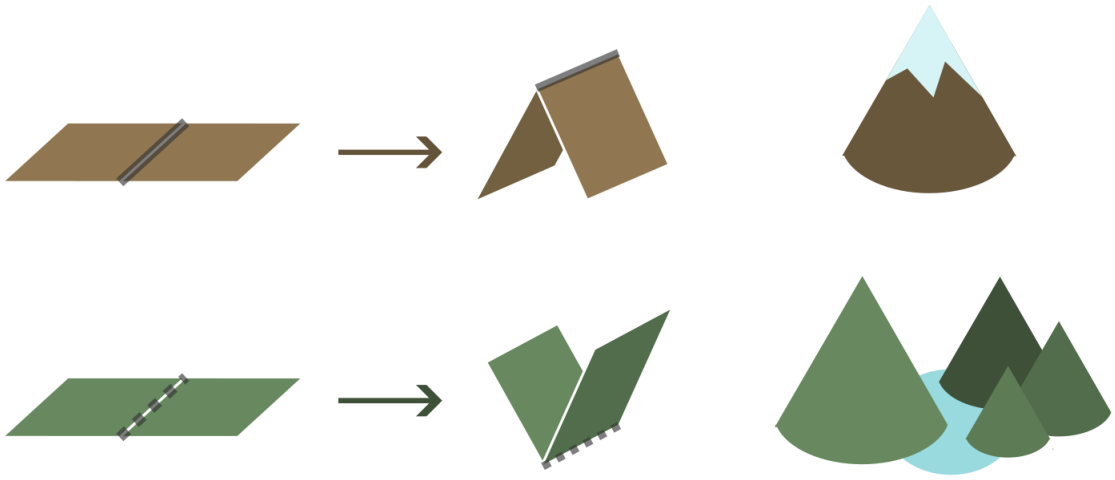

Figure 3.2.1: Mountain and valley folds

Note that all folding diagrams are enumerated up to rotation and reflection.

Theorem 3.2.1. *There exist two folding patterns which close the solo 1-cell fenestration, shown in Figure 3.2.2.*

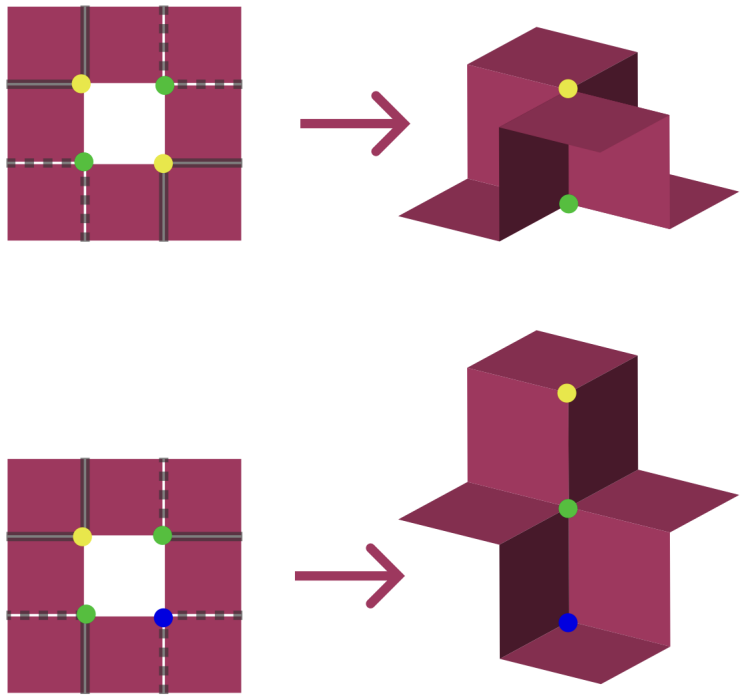

Figure 3.2.2: Folding diagrams depicting both ways to close the solo 1-cell fenestration

Proof. Casework checking each possible assignment of mountain or valley to all 8 hinges would require $\binom{8}{2} = 28$ cases, so our proof instead enumerates all the ways to associate/glue the vertices which surround the fenestration.

Our 1-cell fenestration has 4 vertices. We have 3 cases. Case 1, our folding assignment associates 0 pairs of vertices, and leaves all 4 fixed, then our fenestration is not closed. Case 2, our folding assignment associates 1 pair of vertices, and leaves 2 fixed. Case 3, our folding assignment associates 2 pairs of vertices, and leaves 0 fixed. Cases 2 and 3 effectively collapse our fenestration, and are pictured in 3.2.2. These are unique up to rotation and reflection symmetries. Thus we have exactly 2 valid folding assignments for the width-1 strip surrounding the solo 1-cell fenestration.

□

Theorem 3.2.2. *There exists 1 vertex identification which closes the solo 2-cell fenestration, shown in Figure 3.2.3.*

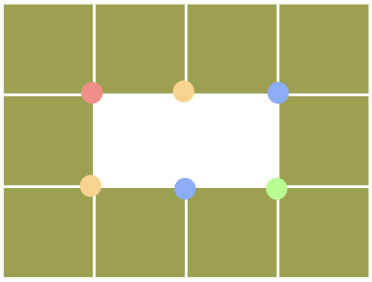

Figure 3.2.3: The vertex identification which closes the solo 2-cell fenestration

Proof. For the 2-cell fenestration, we will similarly enumerate all the ways to pair some vertices and leave others fixed to determine our valid vertex identification pattern. We have six vertices surrounding our fenestration. If we pair none, and leave 6 fixed, our fenestration will not close. If we have one pair, and 4 fixed, our 2-cell fenestration will not close, though we may close one of the two squares. If we have 2 pairs, and 2 fixed, we can close our fenestration, and must now ask how many valid mountain-valley assignments to the surrounding width-1 strip exist which will collapse the fenestration. Having 3 pairs of vertices is impossible. □

Theorem 3.2.3. *There exist at least 6 folding patterns which close the solo 2-cell fenestration.*

Proof. See 6 foldings constructed in Figure 3.2.4 □

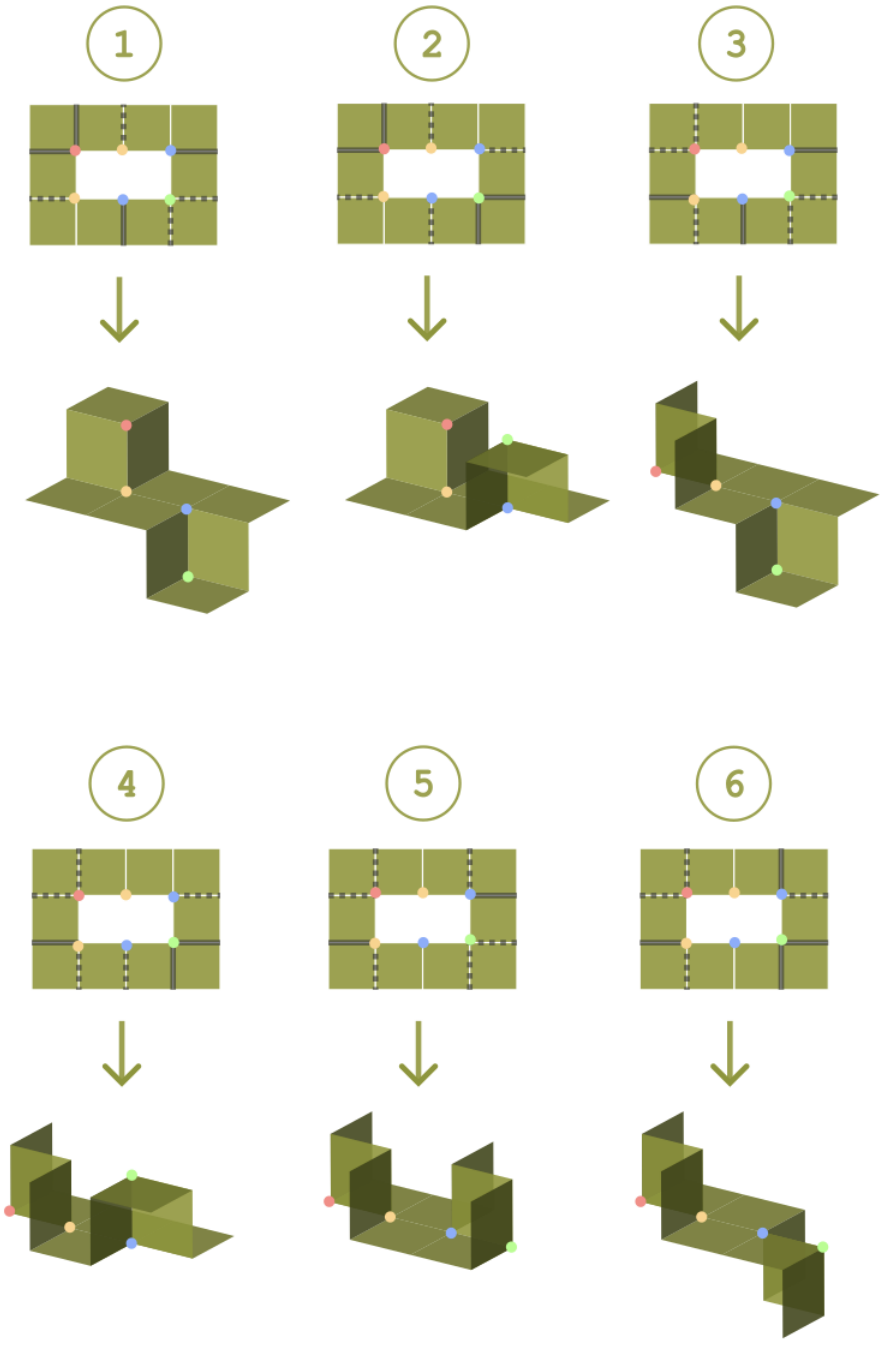

Figure 3.2.4: All 6 foldings which close the solo 2-cell fenestration

Conjecture 3.2.4. *There exist exactly 6 folding patterns which close the solo 2-cell fenestration.*

Thoughts toward a proof of this conjecture are outlined below.

We propose a branching argument to exhaust all folding possibilities.

In Figure 3.2.5 we show that folding #1 may be manipulated in two ways: folded along the orange hinge or blue hinge. If we perform either of these movements, we produce folding #4. If we perform both of these movements, we produce folding #6. No other manipulations of folding #1 are possible.

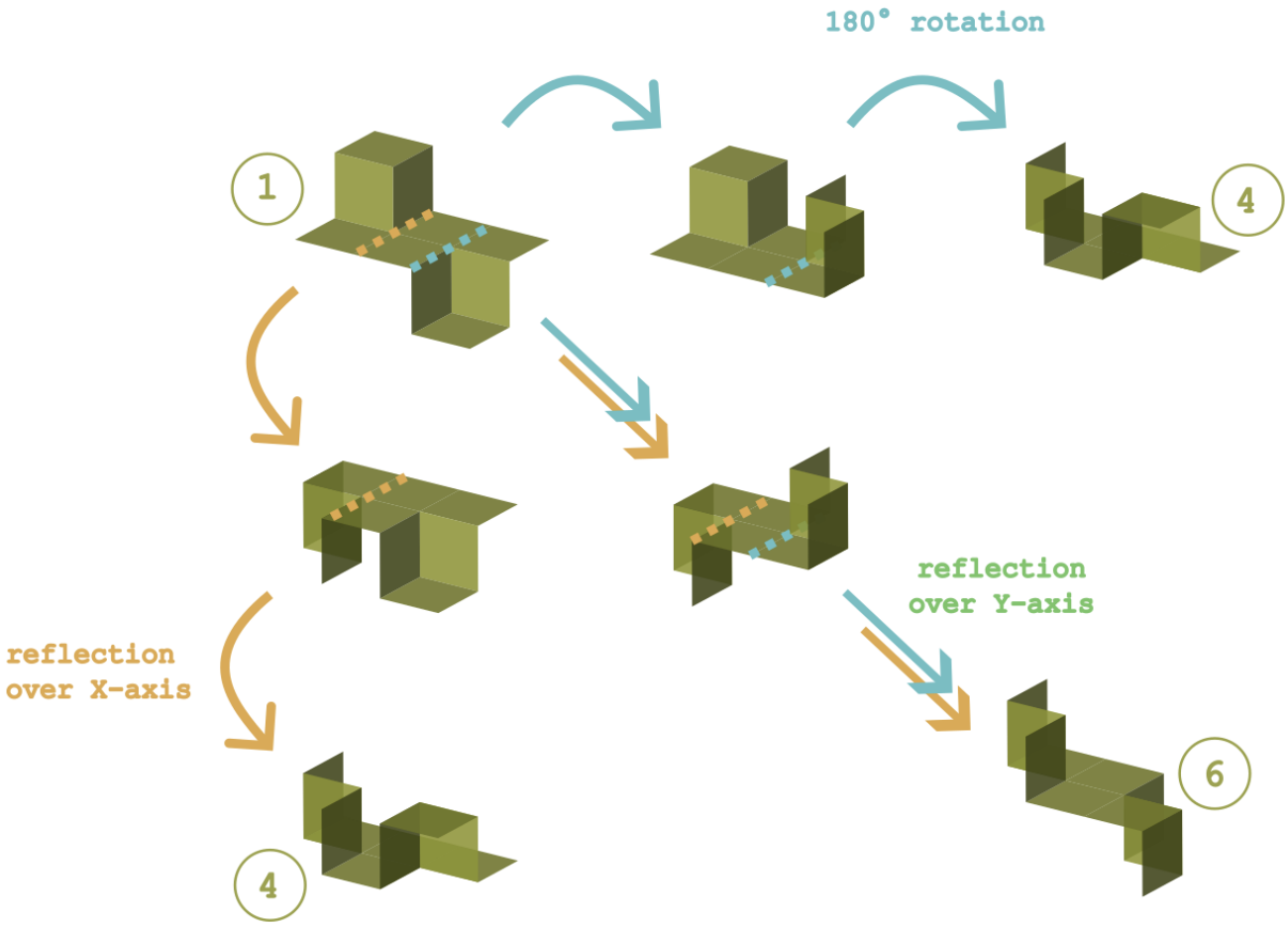

Figure 3.2.5: Closings of the solo 2-cell fenestration which branch from folding #1

In Figure 3.2.6 we show that folding #2 may be manipulated in three ways: folded along the orange, blue, or pink hinge. If we fold along the pink or blue hinge, we produce folding #3. If we fold along orange and blue, we produce folding #5. No other manipulations of folding #2 are possible.

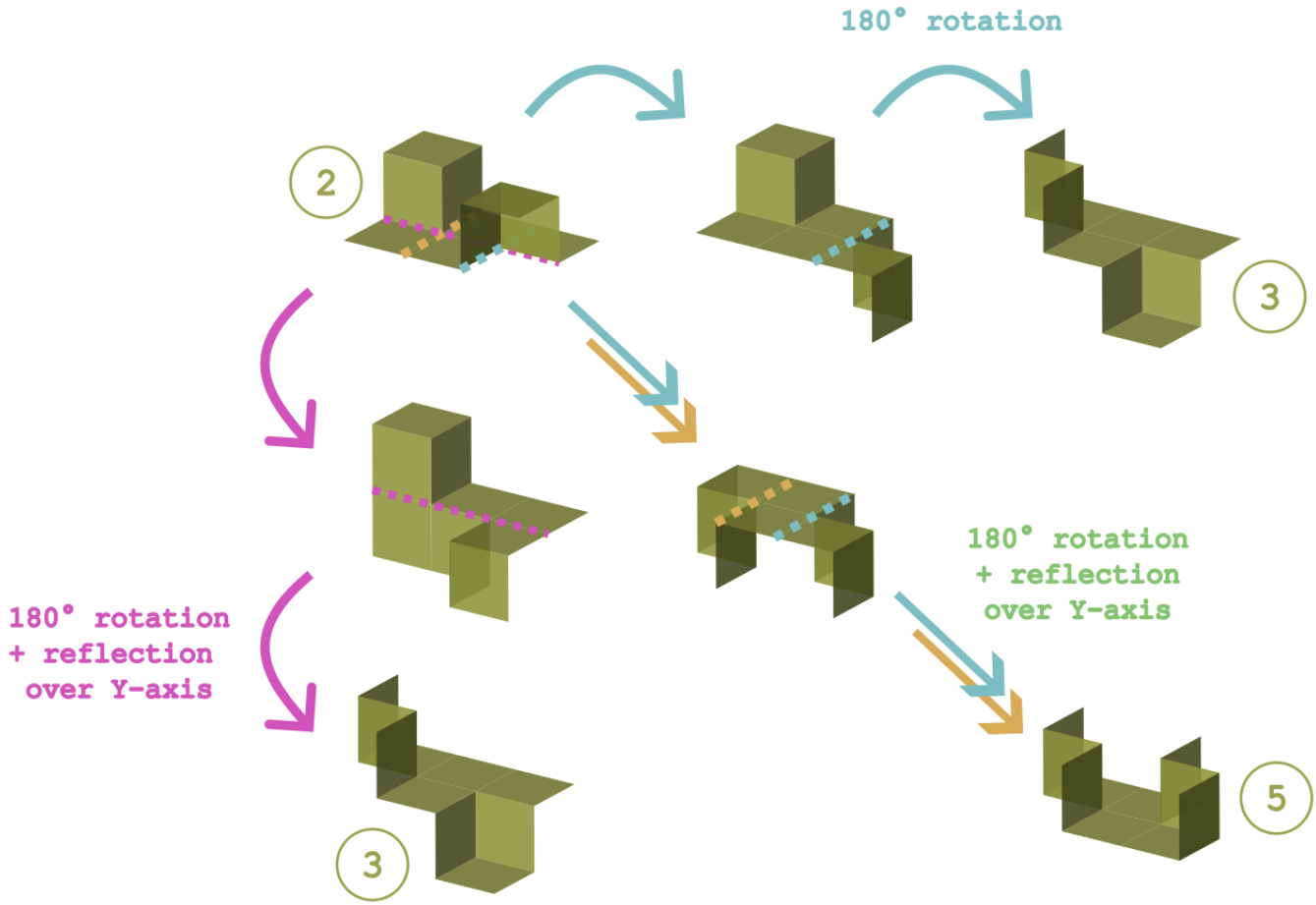

Figure 3.2.6: Closings of the solo 2-cell fenestration which branch from folding #2

We believe the step missing to turn this conjecture into a proof is determining that 1 and 2 are the only starting points for our branching argument.

3.3 From Local to Global: Collapsing Unbounded Fenestrated Polyominoes

We now use our local picture of solo fenestrations to construct collapsible and non-collapsible unbounded polyominoes built from infinite squares.

Definition 3.3.1. An *unbounded fenestrated polyomino* is a fenestrated polyomino built from an infinite number of squares.

Definition 3.3.2. A *periodic pattern* in the plane is a design having the following property: there exists a finite region and two linearly independent translations such that the set of all images of the region when acted on by the group generated by these translations produce the original design.

Definition 3.3.3. An *unbounded periodically fenestrated polyomino* is an unbounded fenestrated polyomino whose fenestrations are arranged in a periodic pattern.

Definition 3.3.4. A *collapsible unbounded periodically fenestrated polyomino* is an unbounded periodically fenestrated polyomino which can be assigned a periodic folding pattern such that its realization as a 3D polyominoid contains zero fenestrations.

We present a collapsible unbounded periodically fenestrated polyomino, built with 1-cell fenestrations, and explicitly construct a folding pattern which collapses all fenestrations. We provide another collapsible unbounded example built with 2-cell fenestrations. Finally, we present a non-collapsible bounded polyomino and explorations in defining non-collapsible unbounded polyominoes. For our non-collapsible unbounded polyomino example, we conjecture it is possible to collapse a maximum of $\frac{1}{2}$ of the fenestrations present.

Future work may include developing techniques to construct collapsible polyominoes using multiple different size fenestrations. We ultimately hope to answer the question: for any given fenestrated polyomino, is it collapsible? And further, if it is collapsible, how many unique folding patterns will collapse it?

3.3.1 A Collapsible Unbounded Periodic Polyomino built with 1-Cell Fenestrations

Before presenting our examples, we must first introduce notation for describing folding patterns and bounded polyominoes.

Definition 3.3.5. A *bounded fenestrated polyomino* of vertical height v and horizontal length h can be described by a $v \times h$ matrix for which a non-zero entry denotes a solid square and a zero entry denotes a transparent square

Example 3.3.6. The bounded fenestrated polyomino described by the $\begin{bmatrix} 1 & 1 \\ 1 & 0 \end{bmatrix}$ matrix is pictured in Figure 3.3.1

Definition 3.3.7. Let P be a bounded fenestrated polyomino. Let v be the vertical height of P and h be the horizontal length of P.

We specify a *folding pattern* on a $v \times h$ polyomino by two matrices V and H, where V is a $v \times (h+1)$ matrix which describes the vertical folds on P and H is a $(v+1) \times h$ matrix which describes the horizontal folds on P.

Entries of the matrix correspond to mountain-valley folds as follows:

- 1 denotes a mountain
- 0 denotes no fold
- -1 denotes a valley

Example 3.3.8. A folding pattern assigned to a 2×2 polyominoid, described by two matrices of sizes 2×3 and 3×2, is pictured in Figure 3.3.1

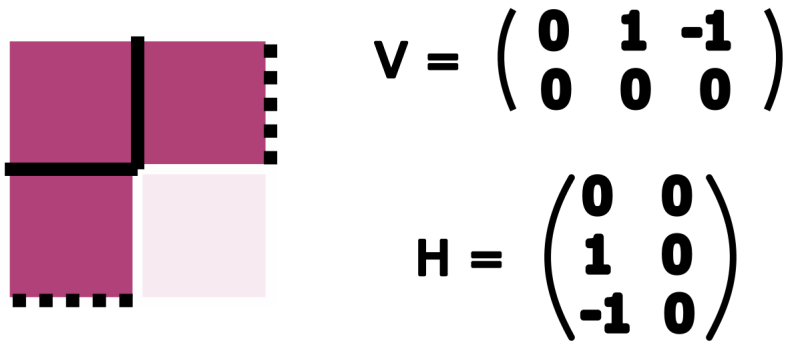

Figure 3.3.1: A folding pattern described by two matrices

Theorem 3.3.9. *There exists a collapsible unbounded periodically fenestrated polyomino built with 1-cell fenestrations.*

Proof. We will explicitly construct our periodic polyomino and folding pattern by defining a finite region and 2 linearly independent translation vectors.

Let the 2D finite region for our periodic polyomino be the $\begin{bmatrix} 1 & 1 \\ 1 & 0 \end{bmatrix}$ polyomino.

Let our 2D translation vectors be $\begin{bmatrix} 2 \\ 0 \end{bmatrix}$ and $\begin{bmatrix} 0 \\ 2 \end{bmatrix}$. This construction is pictured in Figure 3.3.2

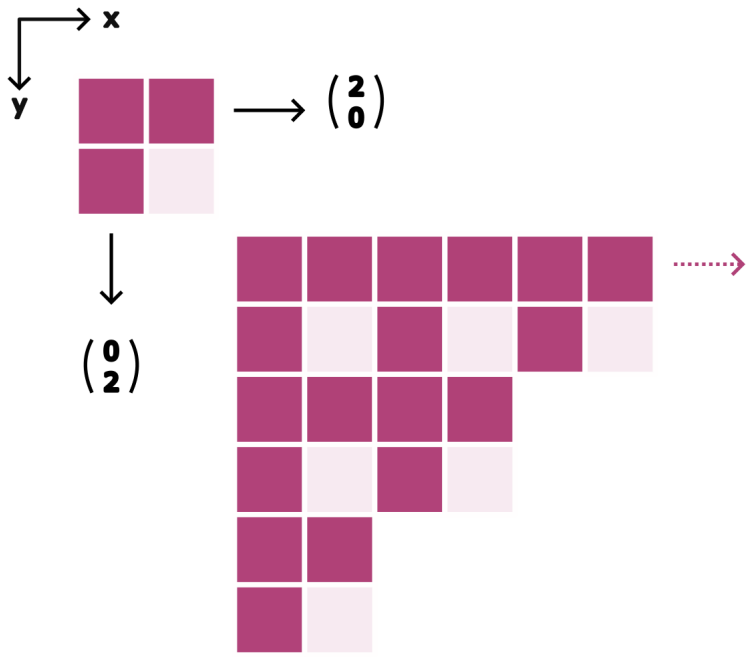

Figure 3.3.2: Construction of an unbounded periodically fenestrated polyomino given a finite region and two translation vectors

We now construct our folding pattern. We specify our folds as follows. $V = \begin{bmatrix} 0 & 1 & -1 \\ 0 & 0 & 0 \end{bmatrix}$ and $H = \begin{bmatrix} 0 & 0 \\ 1 & 0 \\ -1 & 0 \end{bmatrix}$. Observe that our 2D finite region folds to a 3D finite region as pictured in Figure 3.3.3

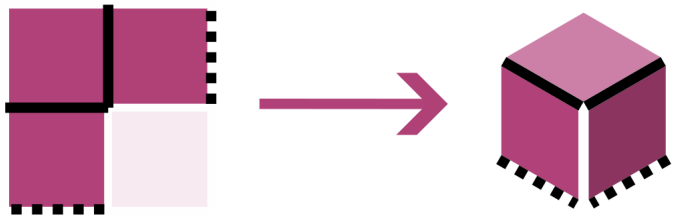

Figure 3.3.3: Folding of 2D finite region into 3D finite region

Let our 3D translation vectors be $\begin{bmatrix} 1 \\ 0 \\ 1 \end{bmatrix}$ and $\begin{bmatrix} 0 \\ 1 \\ 1 \end{bmatrix}$.

A finite expansion of our periodic pattern and its successive folding is shown in Figure 3.3.4

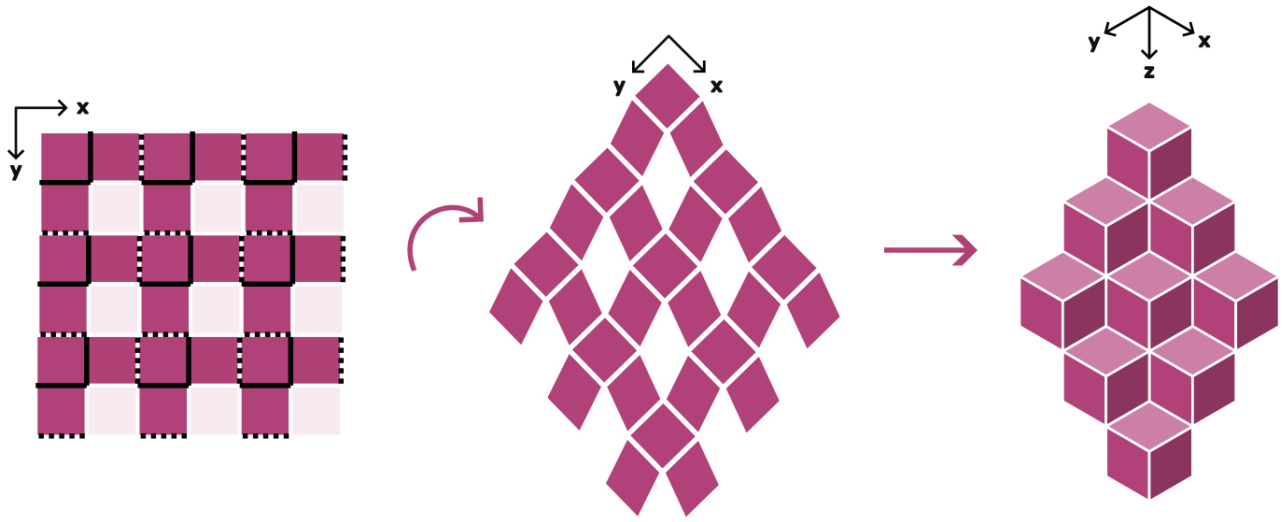

Figure 3.3.4: A finite expansion of the polyomino and folding we constructed

We observe, locally, every fenestration is surrounded by a width-1 border strip of squares which has a folding pattern assignment we proved collapses a 1-cell fenestration in Theorem 3.2.1, shown again in Figure 3.3.5

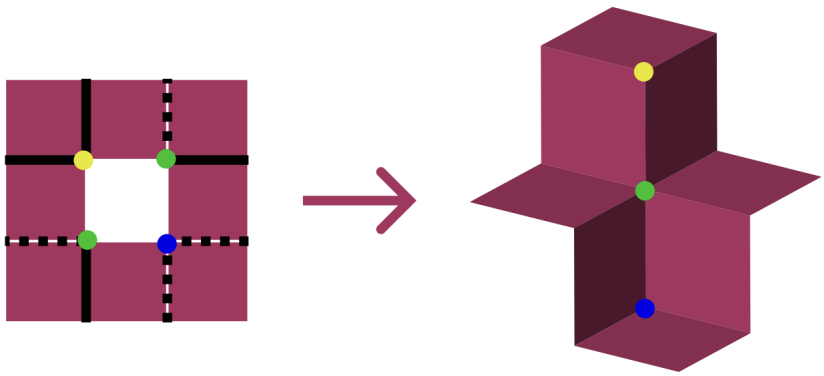

Figure 3.3.5: A collapsing of a solo 1-cell fenestration

Thus the unbounded periodically fenestrated 2D polyomino we constructed collapses to a non-fenestrated 3D polyominoid.

□

Theorem 3.3.10. *There exists an embedding function $f : 2\mathbb{Z}^2 \to \mathbb{Z}^3$ which explicitly maps our fenestrated 2D polyomino to our non-fenestrated 3D polyominoid.*

Proof. We label the top-left-vertex of each square which lies diagonally adjacent to a fenestration, and construct an explicit function which maps this vertex to a its new position in 3-space after folding. This vertex labeling is illustrated in Figure 3.3.6

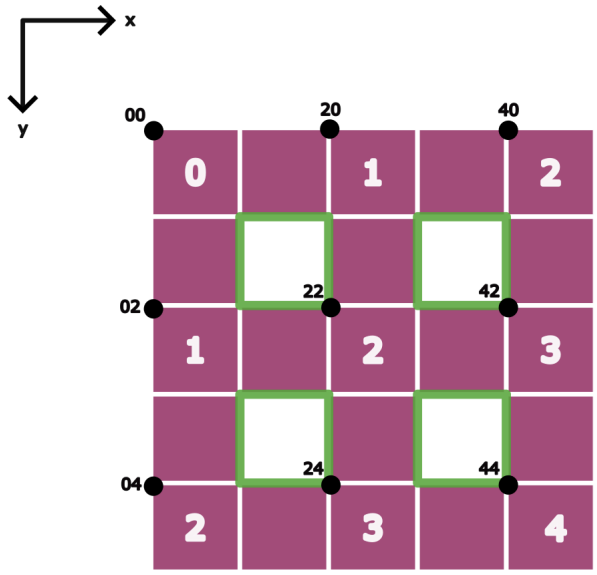

Figure 3.3.6: Vertex labeling

In Figure 3.3.7 we rotate our perspective and begin our folding process, to demonstrate how the z-values, labeled on the faces of the squares, become apparent.

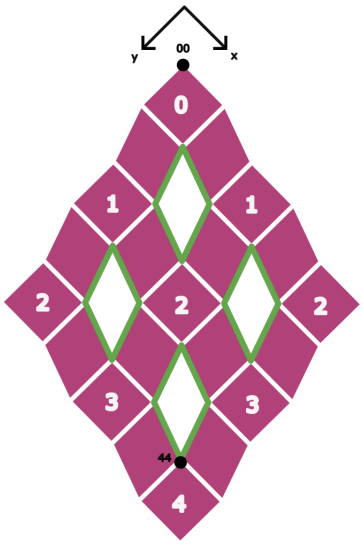

Figure 3.3.7: Beginning our folding process

Finally, we fully collapse our fenestrated 2D polyomino into a 3D non-fenestrated polyominoid, and relabel our vertices in Figure 3.3.8.

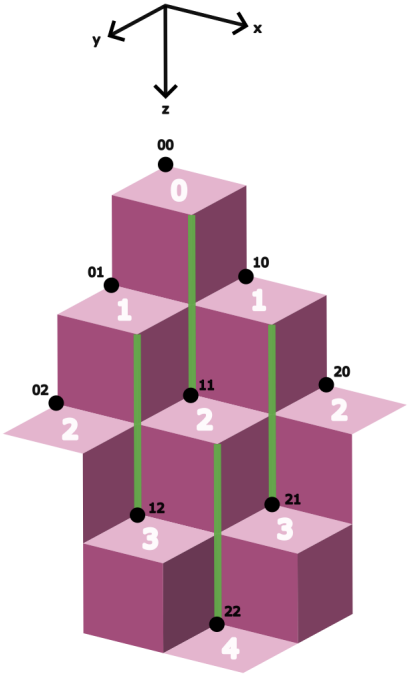

Figure 3.3.8: Fully collapsed, non-fenestrated 3D polyominoid

Let $f : 2\mathbb{Z}^2 \to \mathbb{Z}^3$ be defined by $f(x, y) = (\frac{x}{2}, \frac{y}{2}, \frac{x+y}{2})$.

See Figures 3.3.6 and 3.3.8 to check that $(0,0)$ maps to $(0,0,0)$, and $(2,2)$ maps to $(1,1,1)$, and $(4,2)$ maps to $(2,1,3)$, etc.

3.3.2 A Collapsible Unbounded Periodic Polyomino built with 2-Cell Fenestrations

Theorem 3.3.11. *There exists a collapsible unbounded polyomino built with 2-cell fenestrations.*

Proof. Let our 2D finite region be $\begin{bmatrix} 1 & 1 & 1 \\ 1 & 0 & 0 \end{bmatrix}$, pictured in Figure 3.3.9

Figure 3.3.9: Our finite region

Let our folding pattern be given by $V = \begin{bmatrix} 0 & 1 & -1 & 0 \\ 0 & 0 & 0 & 0 \end{bmatrix}$ and $H = \begin{bmatrix} 0 & 0 & 0 \\ 1 & 0 & 0 \\ -1 & 0 & 0 \end{bmatrix}$, shown in Figure 3.3.10

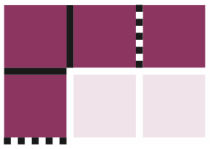

Figure 3.3.10: Our folding assignment

Let our 2D translation vectors be $\alpha = \begin{bmatrix} 3 \\ 0 \end{bmatrix}$ and $\beta = \begin{bmatrix} 1 \\ 2 \end{bmatrix}$. Our finite region after applying α, β, and $\alpha + \beta$ is pictured in Figure 3.3.11

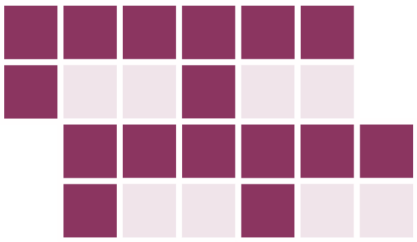

Figure 3.3.11: Our finite region translated by α, β, and $\alpha + \beta$

Observe our 2D finite region folds to the 3D polyominoid shown in Figure 3.3.12. This is our 3D finite region, we nickname it the "hat."

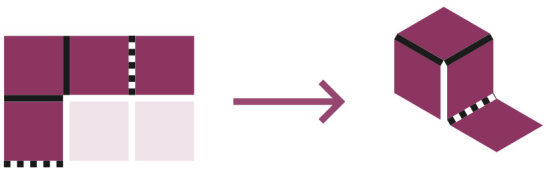

Figure 3.3.12: Folding our 2D finite region into our 3D finite region

Let our 3D translation vectors be $a = \begin{bmatrix} 2 \\ 0 \\ 1 \end{bmatrix}$ and $b = \begin{bmatrix} 1 \\ 1 \\ 1 \end{bmatrix}$. See our 3D finite region translated by a, b, and $a+b$ in Figure 3.3.13. Observe that this is precisely the object we obtain by folding our 2D finite region expanded by α, β, and $\alpha + \beta$, pictured in Figure 3.3.11

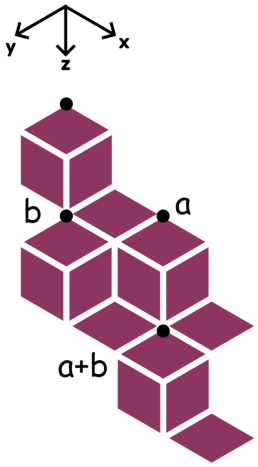

Figure 3.3.13: Our 3D finite region translated by a, b, and $a + b$

Observe that 0, a, b, and $a + b$ form a parallelogram R. There exists a plane P spanned by a and b on which this parallelogram lies. Let L be the lattice defined by a and b. We can tile this plane P with by placing copies of R with vertices on our lattice points in L. Below each lattice point hangs a "hat." The union of these hats forms an unbounded non-fenestrated polyominoid.

□

3.3.3 A Non-Collapsible Bounded Fenestrated Polyomino

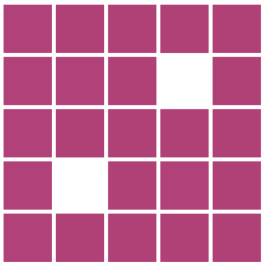

Figure 3.3.14: A non-collapsible bounded polyomino

Theorem 3.3.12. *It is impossible to fully collapse both fenestrations in the* $\begin{bmatrix} 1 & 1 & 1 & 1 & 1 \\ 1 & 1 & 1 & 0 & 1 \\ 1 & 1 & 1 & 1 & 1 \\ 1 & 0 & 1 & 1 & 1 \\ 1 & 1 & 1 & 1 & 1 \end{bmatrix}$ *bounded polyomino pictured in Figure 3.3.14*

Proof. From Theorem 3.2.1, we know there exist exactly two foldings which close a 1-cell fenestration.

We pick one of our fenestrations and apply folding #1. We see that the rest of the polyomino is paralyzed by this folding, and no further folding assignments are possible. Thus it is impossible to close the second fenestration.

This is true for folding #2 as well. Both foldings are illustrated in Figure 3.3.15.

Thus our bounded fenestrated polyomino is non-collapsible.

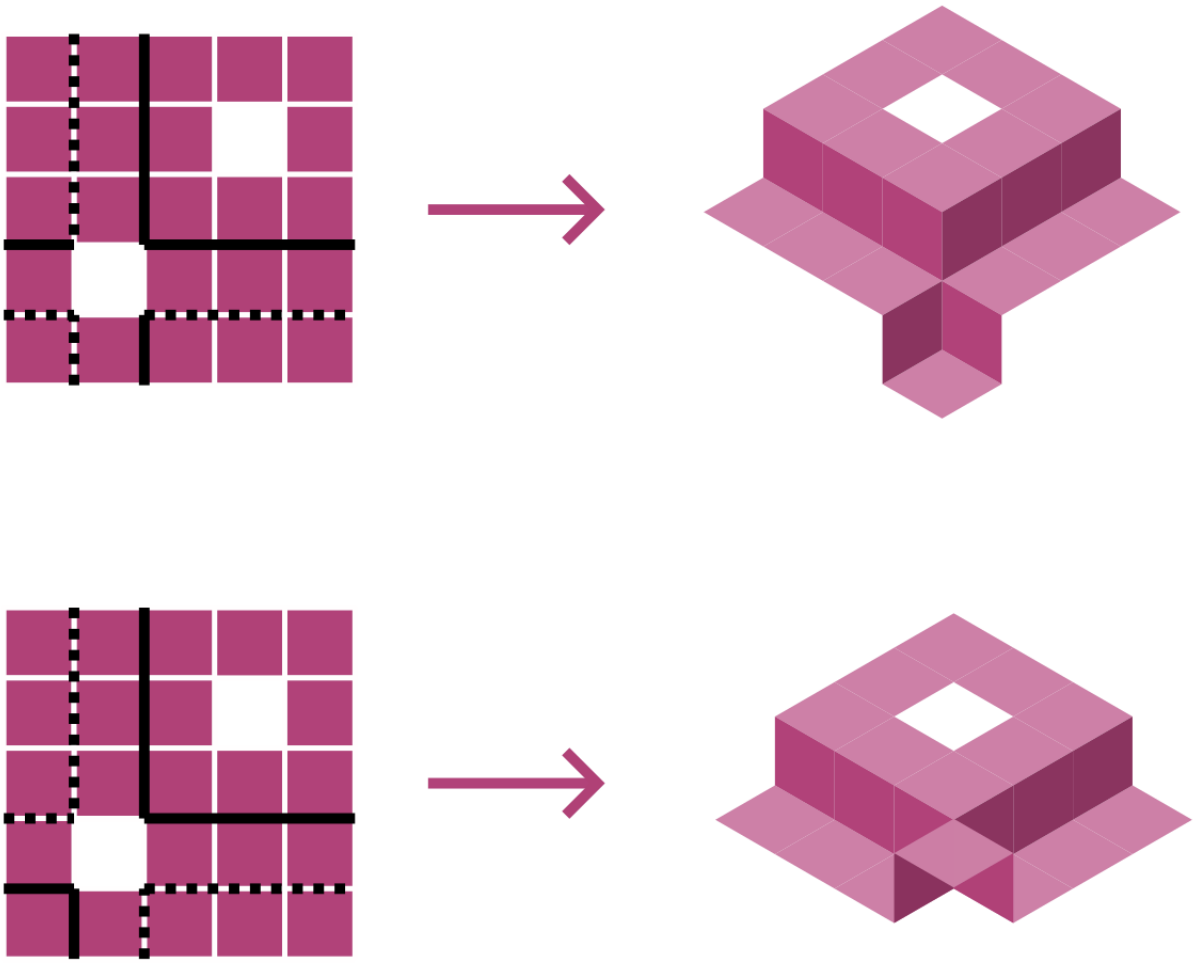

Figure 3.3.15: Illustration of second fenestration being paralyzed open

□

3.3.4 A Non-Collapsible Unbounded Periodically Fenestrated Polyomino

Figure 3.3.16: A subset of an unbounded periodically fenestrated polyomino

Conjecture 3.3.13. *We can collapse a maximum of $\frac{1}{2}$ of the fenestrations present in the unbounded periodically fenestrated polyomino generated by finite region* $\begin{bmatrix} 1 & 1 & 1 & 1 \\ 1 & 1 & 1 & 0 \\ 1 & 1 & 1 & 1 \\ 1 & 0 & 1 & 1 \end{bmatrix}$ *and translation vectors* $\begin{bmatrix} 4 \\ 0 \end{bmatrix}$ *and* $\begin{bmatrix} 0 \\ 4 \end{bmatrix}$*, pictured in Figure 3.3.16*

4
Embedding Geometrized Chromotopologies in 3-Space

4.1 Intro to Adinkra Chromotopologies

In this chapter, we introduce Adinkra chromotopologies, which are a special class of N-regular, edge-N-colored bipartite graphs which encode information about objects from supersymmetry physics, introduced in physics by Faux and Gates in 2005 in [FG05]. This concept was mathematically formalized by Doran et. al. in [CS1D].

Definition 4.1.1. A *bipartite graph* is a graph whose vertices are partitioned into two disjoint sets (which we label white and black) such that every edge connects a white vertex to a black vertex.

Definition 4.1.2. An *N-regular* graph has N edges incident to every vertex.

Definition 4.1.3. An *edge-N-colored* graph has N colors assigned to its edges.

Definition 4.1.4. An N-dimensional Adinkra *topology* is a finite connected simple graph G such that G is bipartite and N-regular (every vertex has exactly N incident edges).

Definition 4.1.5. An N-dimensional Adinkra *chromotopology* is a topology G such that the following holds:

1. Edges of G are colored by N colors, such that every vertex is incident to exactly one edge of each color.

2. For any distinct i and j, the edges in $E(G)$ with colors i and j form a disjoint union of 4-cycles.

It is known, from [CS1D], that hypercubes quotiented by doubly even codes index Adinkra chromotopologies.

Definition 4.1.6. A *doubly even code* is a subspace of $\mathbb{F}_2^N$ such that, for each element in the subspace (i.e. each N-digit sequence of 0's and 1's, or "codeword"), the number of non-zero digits in the codeword is divisible by 4.

N-cubes, pictured in Figure 4.1.1, are particularly useful examples of chromotopologies.

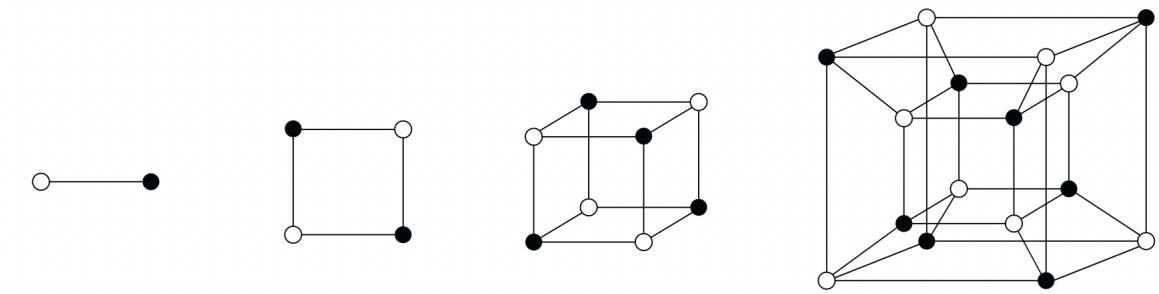

Figure 4.1.1: Topologies (i.e. 1-skeletons) of the 1-cube, 2-cube, 3-cube, and 4-cube

The *N-Cube* has 2^N vertices which we label 0 to $2^N - 1$ in binary. We join vertices which differ in exactly one bit.

Example 4.1.7. The vertices labeled 1011 and 1111 will be joined by an edge because they differ in only the 2nd coordinate. The vertices labeled 1110 and 1000 will not be joined by an edge because they differ in both the 2nd and 3rd coordinate.

Each label is an N-digit bit string, and each edge incident to a vertex corresponds to a bit change, so the graph must be N-regular.

Example 4.1.8. The vertex 111 in the 3-cube is adjacent to exactly 3 vertices $\{011, 101, 110\}$.

We can endow this graph with a natural bipartite white/black coloring of its vertices by using a weight function.

Definition 4.1.9. The *weight* of a vertex is the number of 1's in its label.

We color all vertices with even weight white and vertices with odd weight black. Below, in Figure 4.1.2, we have the 1-cube, 2-cube, and 3-cube with vertices labeled as described above.

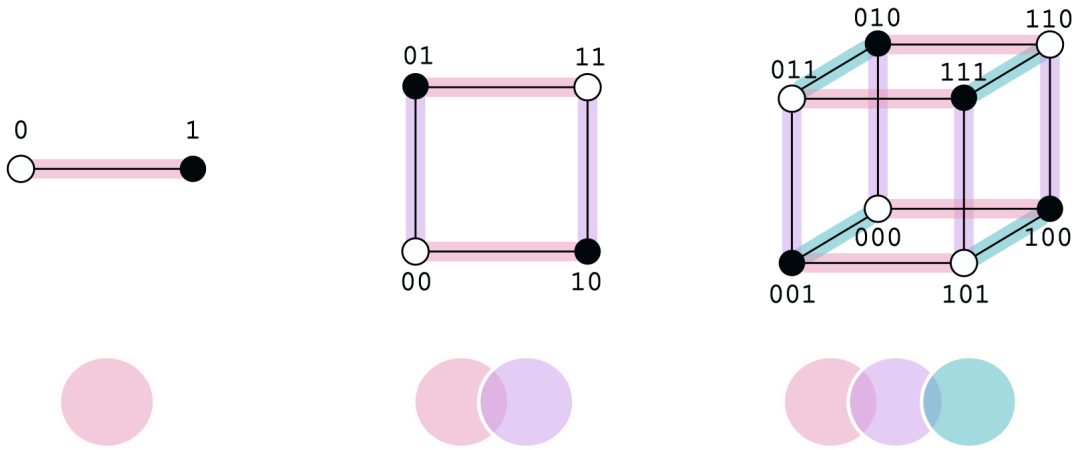

Figure 4.1.2: The 1-cube, 2-cube, and 3-cube with vertices labeled and edges colored.

Definition 4.1.10. A *rainbow* is a choice of cyclic ordering of the colors of a edge-colored graph.

To determine the coloring of the edges of an Adinkra, we construct a "rainbow" by associating the numbers 1 through N with different colors. Let $k \in \{1, 2, ..., N\} \subseteq \mathbb{N}$. Each edge connects two vertices which differ in the kth coordinate, so we assign that edge the kth color in the rainbow. In figure 4.1.3 below, we see the 4-cube with rainbow (pink, purple, blue, green) assigned to edges which swap the 1st, 2nd, 3rd, and 4th coordinate, respectively. This coloring technique is also illustrated for lower dimensions in Figure 4.1.2.

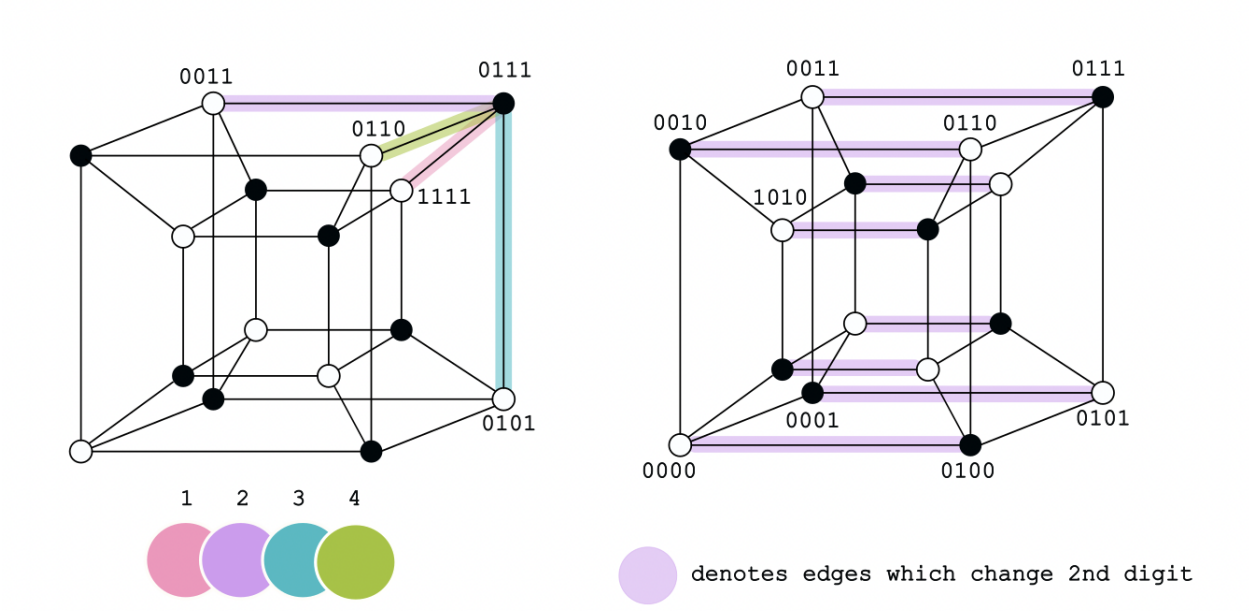

Figure 4.1.3: A rainbow assignment of edge-coloring on the 4-cube

4.2 From Cubes to Riemann Surfaces

In [GSA1], Chuck Doran et. al. describes how an Adinkra chromotopology canonically defines a Riemann surface. First, we map from chromotopologies to ribbon graphs. Then, we use the Grothendiek correspondence as described in [MP98] to map from ribbon graphs to Riemann surfaces.

Definition 4.2.1. A *ribbon graph* is a connected graph that assigns to each vertex of the graph a cyclic permutation of the half edges adjacent to it.

We map from chromotopologies (a graph with vertex bipartition and edge-coloring) to ribbon graphs by assigning the rainbow cyclic order to black vertices, and the reverse of the rainbow cyclic order to white vertices.

Definition 4.2.2. A *manifold* is a topological space which locally resembles Euclidean space near each point.

Definition 4.2.3. A *surface* is a two-dimensional manifold.

Definition 4.2.4. A *singularity* is a point at which a given mathematical object ceases to be well-behaved.

Remark 4.2.5. A surface must not contain singularities. In the context of polyhedral surfaces, this means we must not have more than two faces incident to any given edge.

We want to realize hypercubes as surfaces, but encounter the issue that too many faces meet at each edge, creating singularities. To realize a surface, we remove some faces, so that each edge has exactly two incident faces. How do we consistently pick two faces for each edge? The rainbow coloring of our cube provides us with an elegant answer.

The Grothendiek correspondence allows us to map from ribbon graphs to topological surfaces. The surface is built by using the ribbon graph as a 1-skeleton and filling in only the 2-cells which follow the cyclic ordering of the rainbow. Meaning, faces bordered by (pink, purple), (purple, blue), (blue, green), or (green, pink) edges are all valid, and faces bordered by (pink, blue) or (purple, green) must be removed. Of the 24 faces in the 4-cube, 16 are valid following our rainbow, and 8 must be removed. These valid faces are pictured in Figures 4.2.1 4.2.2 and invalid faces are pictured in Figure 4.2.3.

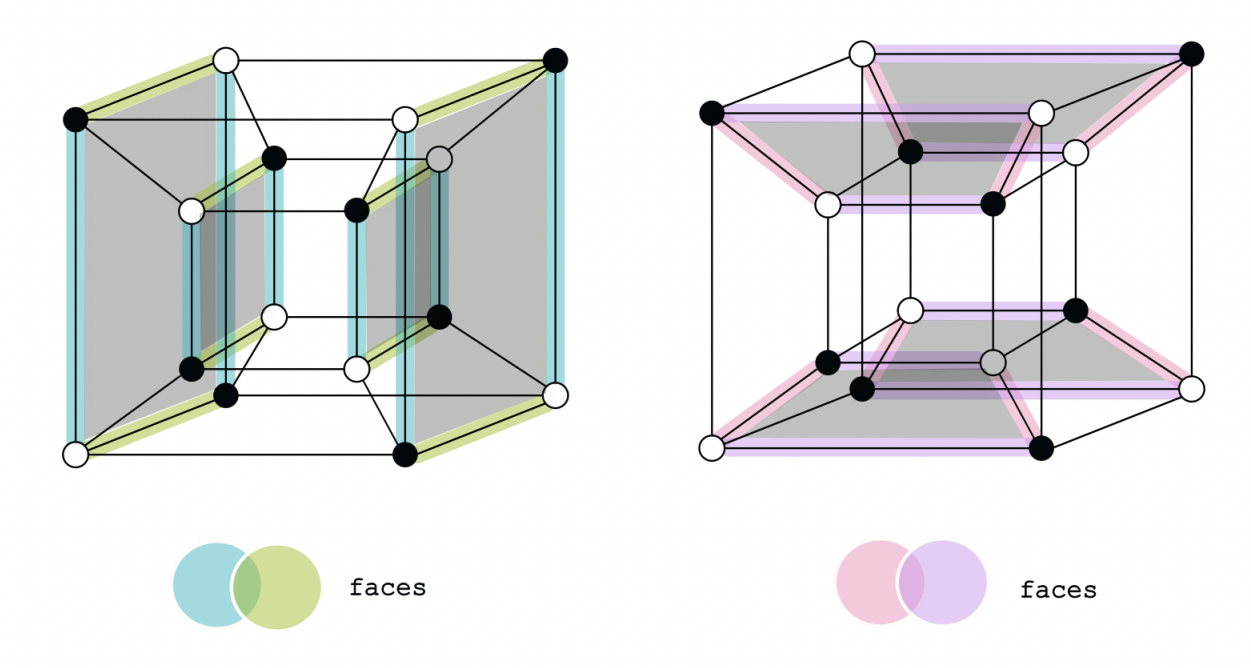

Figure 4.2.1: Selecting 8 of 16 total valid 2-cells according to rainbow

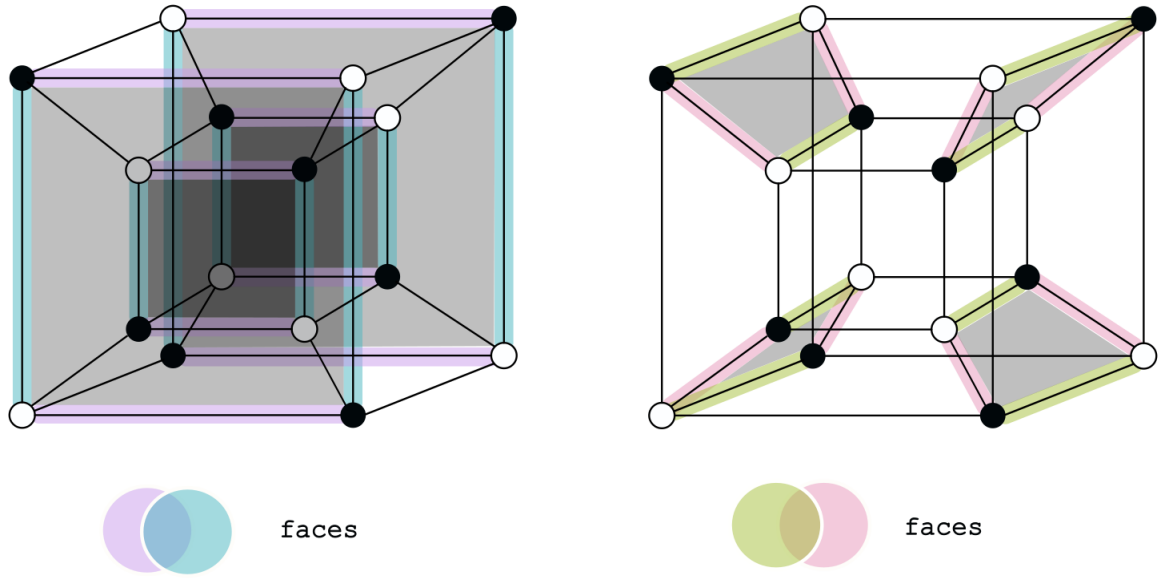

Figure 4.2.2: Selecting remaining 8 of 16 total valid 2-cells according to rainbow

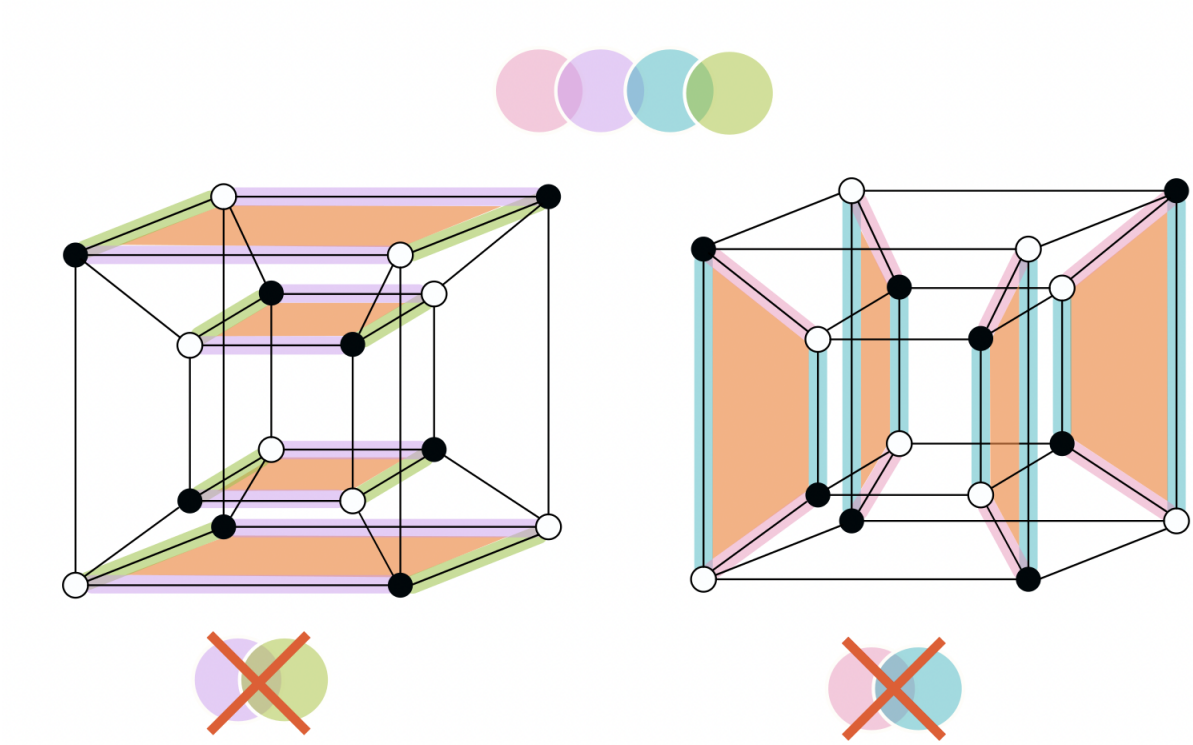

Figure 4.2.3: Invalid faces of the 4-cube according to our rainbow

We ultimately realize a torus. Note this model has been rotated to show the hole more clearly; the through-hole would go top-to-bottom if the above construction is followed precisely, as opposed to front-to-back as shown in Figure 4.2.4 below.

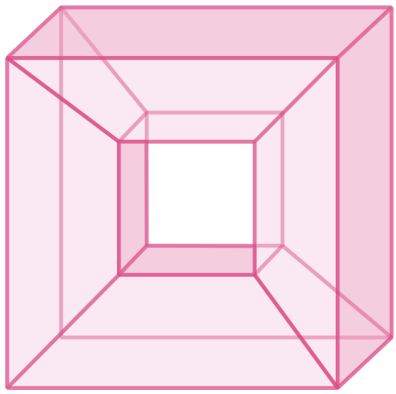

Figure 4.2.4: The 4-cube realized as a Riemann surface using its chromotopology

We can use Euler's formula $\chi = V - E + F$ and the genus formula $\chi = 2 - 2g$ to check that the 4-cube Adinkra is topologically a torus. Typically, a 4-cube would have 16 vertices, 32 edges, and 24 faces. But we have removed 8 faces deemed invalid by the rainbow coloring, which leaves us with 16 valid faces. Thus $\chi = 16 - 32 + 16 = 0$ which gives us $g = 1$, a torus.

4.3 Quotienting Hypercubes

In 2011, Chuck Doran et. al. showed Adinkra chromotopologies can be indexed by colored N-cubes quotiented by doubly even codes in [CS1D].

Definition 4.3.1. A *doubly even code* is a subspace of $\mathbb{F}_2^N$ such that, for each element in the subspace (i.e. each N-digit sequence of 0's and 1's, or "codeword"), the number of non-zero digits in the codeword is divisible by 4.

Below, in Figure 4.3.1, we quotient the 4-cube by the code generated by 1111 (the only doubly even code for N=4). Every vertex is paired with another which together add (mod 2) to 1111. This vertex association results in all edges and faces being paired as well.

Example 4.3.2. The vertex 0110 and the vertex 1001 are both labeled yellow in Figure 4.3.1 because $0110 + 1001 = 1111$.

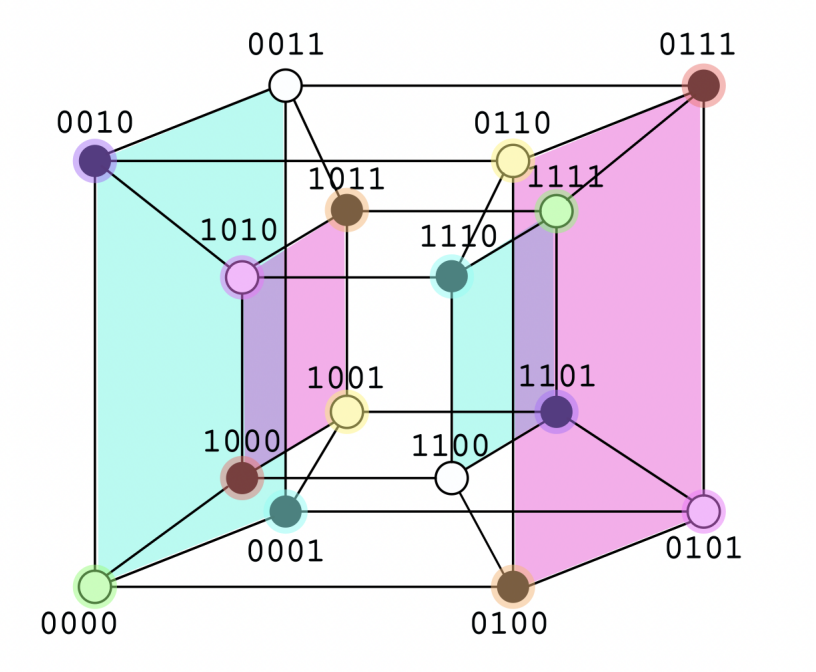

Figure 4.3.1: The 4-cube quotiented by the code generated by 1111

An easy way to determine a vertex's pair without labeling the entire cube is to traverse a path on the cube which follows 4 edges, one corresponding to each basis vector, as shown below in Figure 4.3.2. This works because each color corresponds to flipping a distinct digit in the 4-digit binary code, so traversing a path of length 4 of 4 unique colors will flip all digits of the code of the original vertex.

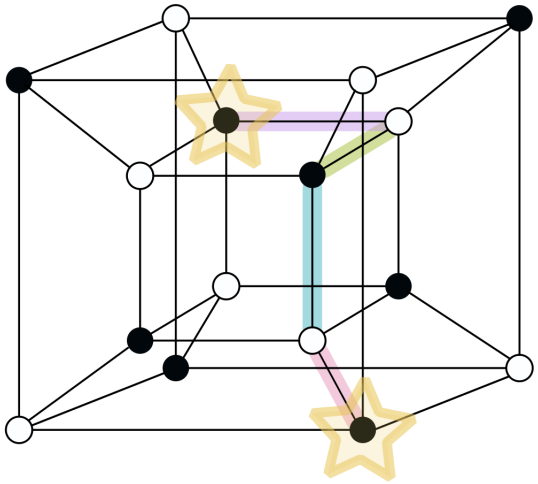

Figure 4.3.2: A length 4 path between a pair of vertices associated by the code generated by 1111

When we quotient the graph of the 4-cube by the code generated by 1111, we obtain a graph of 8 vertices and 16 edges. The 1-skeleton is shown below in Figure 4.3.3, and in the following section we prove it cannot be realized in $\mathbb{R}^3$ using non-intersecting quadrilateral flats to fill in faces.

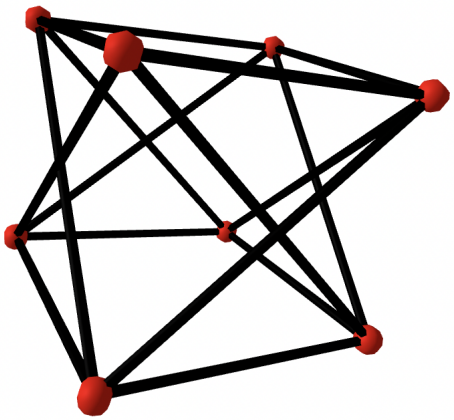

Figure 4.3.3: (4,1) Adinkra

We can use Euler's formula to show the 4-cube quotiented by the code generated by 1111, which we will refer to as the (4,1) chromotopology, is also topologically a torus. The 4-cube

chromotopology has 16 vertices, 32 edges, and 16 faces. Under the quotienting operation, all of these values are halved, so we have $\chi = 8 - 16 + 8 = 0$ which gives us $g = 1$, a torus.

We conjecture the 5-cube quotiented by the code generated by 01111 (the only doubly even code of length 5 up to permutation), while topologically a 3-holed torus, is also unembeddable in $\mathbb{R}^3$ with non-intersecting quadrilateral flats. Its one skeleton is pictured in Figure 4.3.4, a graph of 16 vertices and 40 edges. An analog of our proof for the 4-cube is ineffective for the 5-cube and will require more advanced techniques.

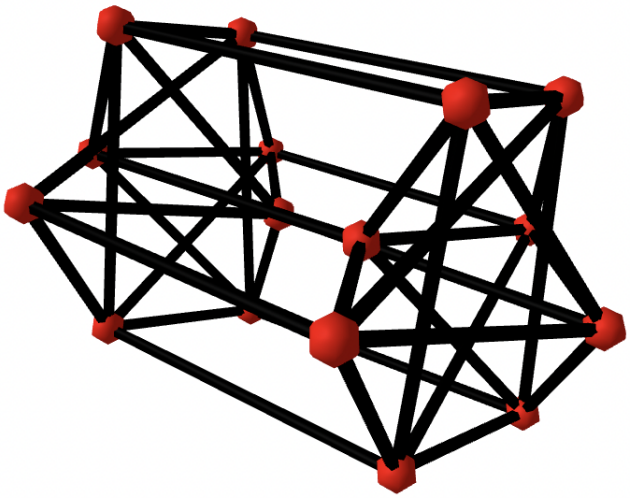

Figure 4.3.4: (5,1) Adinkra

4.4 Embeddability of N=4 Chromotopologies

In this section, we describe the embeddability of the 4-dimensional chromotopologies using non-intersecting quad flats.

A note about notation: the (4,0) chromotopology refers to the 4-cube and the (4,1) chromotopology refers to the 4-cube quotiented by the code generated by 1111.

Theorem 4.4.1. *The (4,0) chromotopology is embeddable in* $\mathbb{R}^3$ *using non-intersecting quad flats.*

Proof. The classically known tesseract picture which is shown in many figures throughout this paper including Figure 4.3.2, is a valid embedding of the 4-cube into $\mathbb{R}^3$ using non-intersecting quad flats. □

Theorem 4.4.2. *The (4,1) chromotopology is not embeddable in* $\mathbb{R}^3$ *using non-intersecting quad flats.* .

Before we begin the proof, note that the 4-dimensional hypercube has 16 vertices, and once quotiented by code generated by 1111, which associates pairs of vertices such as 1011 and 0100, the (4,1) chromotopology must have exactly 8 vertices.

Proof. This proof is illustrated visually in Figure 4.4.1. Let v_1 be a vertex in the (4,1) chromotopology. This vertex has valence 4 by definition, so let us attach 4 quads as petals, as shown in step 1 of the figure. The structure of the N-cube demands these petals must fold up to meet each other, as shown in step 2. We observe these quads meet each other at 4 additional vertices, we label v_2, v_3, v_4, v_5 in step 3. We also see each quad has one remaining vertex unlabeled, we label v_6, v_7, v_8, v_9 in step 4. We have surpassed our limit of 8 vertices and therefore it is impossible to embed the (4,1) chromotopology in $\mathbb{R}^3$. □

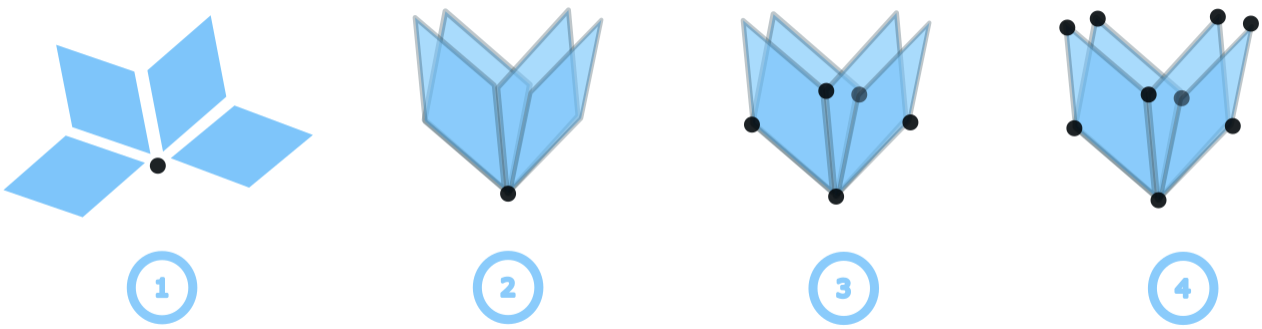

Figure 4.4.1: Visual proof of Theorem 4.4.2

Appendix A
Constructing a Physical Model of the n=4 Configuration Space

While visiting the Max Planck Institute for Mathematics in the Sciences in Leipzig, Germany, in January 2024, to conduct research under Erika Roldan, I had great fun constructing a physical model of $\mathbb{G}_4$, the mechanical configuration space for $n = 4$ polyominoids, which lives on my office door. Paper folding is a passion of mine and it brought me much joy to create this model as a part of my problem solving process.

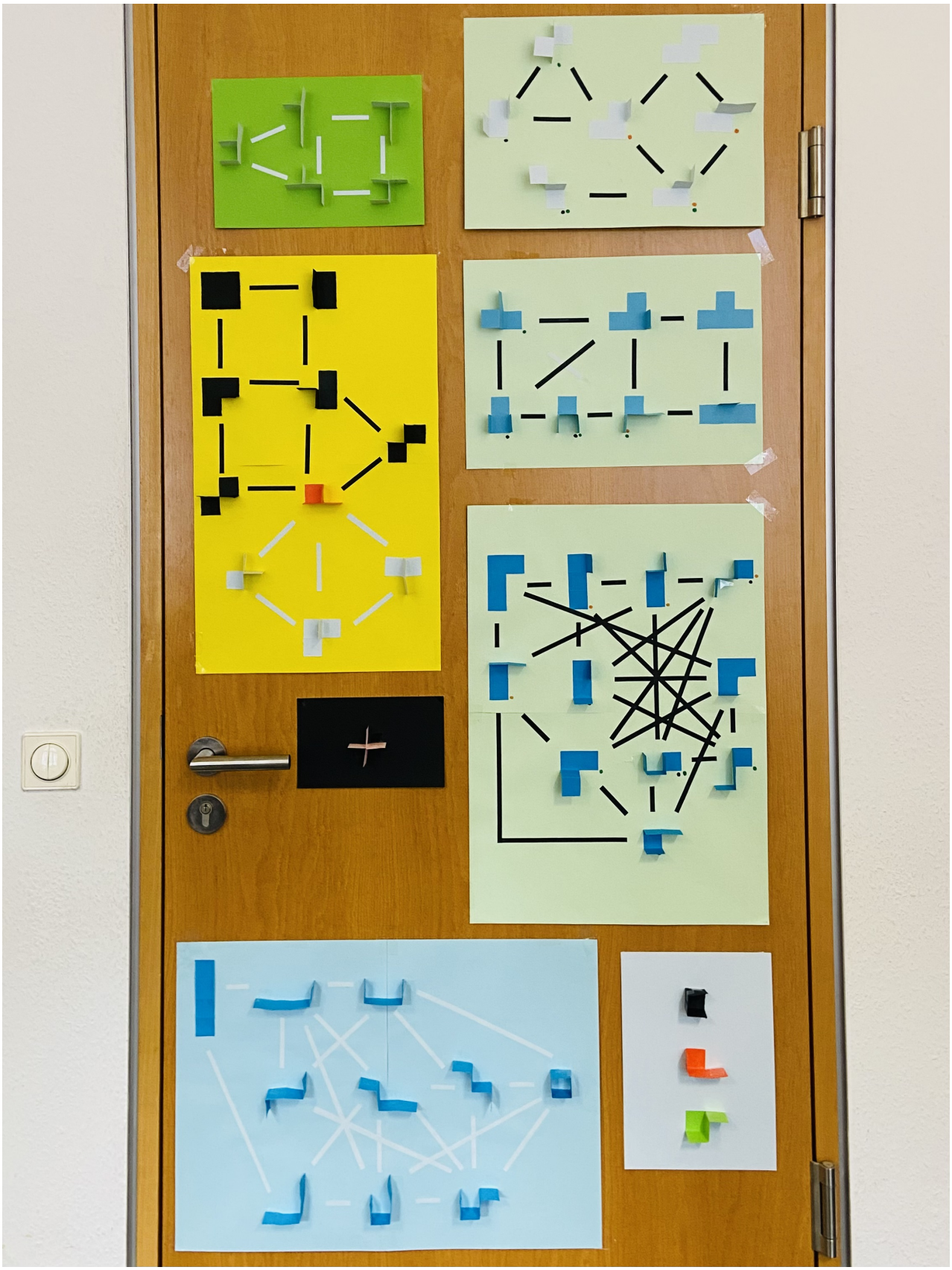

Bibliography

[MC18] Minako Chinen, *Geometric and Graphical Study of 1-Dimensional N-Extended Supersymmetry Algebras* (2018), available at https://era.library.ualberta.ca/items/c5097c8d-7299-44d6-8319-5d53dc7667d0.

[MP98] Motohico Mulase and Michael Penkava, *Ribbon Graphs, Quadratic Differentials on Riemann Surfaces, and Algebraic Curves Defined over Q* (1998), available at https://www.math.ucdavis.edu/~mulase/texfiles/ribbon.pdf.

[CS1D] Charles Doran, Michael Faux, Jim Gates, Tristan Hübsch, Kevin Iga, Greg Landweber, and Robert Miller, *Codes and Supersymmetry in One Dimension* (2011), available at https://arxiv.org/abs/1108.4124.

[GSA1] Charles Doran, Kevin Iga, Jordan Kostiuk, Greg Landweber, and Stefan Méndez-Diez, *Geometrization of N-Extended 1-Dimensional Supersymmetry Algebras, I* (2015), available at https://arxiv.org/abs/1311.3736.

[FG05] S. J. Gates Jr Michael Faux, *Adinkras: A Graphical Technology for Supersymmetric Representation Theory* (2005), available at https://arxiv.org/abs/hep-th/0408004.

[ME61] Murray Eden, *A two-dimensional growth process* (1961), available at https://digitalassets.lib.berkeley.edu/math/ucb/text/math_s4_v4_article-15.pdf.

[SG94] Solomon Golomb, *Polyominoes: Puzzles, Patterns, Problems, and Packings*, Princeton University Press, 1994.

[YZ11] Yan X Zhang, *Adinkras for Mathematicians* (2011), available at https://arxiv.org/pdf/1111.6055.